The localization of chitin synthase mediates the patterned deposition of chitin in developing Drosophila bristles.

Paul N. Adler

Biology Department

Cell Biology Department

University of Virginia

Charlottesville, VA 22904

Abstract

The insect exoskeleton is a morphologically complex structure that is a key for the life style of this very successful group of animals. The cuticular cytoskeleton contains proteins, lipids and the N-acetyl glucosamine polymer chitin. Chitin is a highly patterned and essential component of the insect exoskeleton synthesized by chitin synthase. In most body regions chitin fibrils are found in a stack of parallel arrays that can be detected by transmission electron microscopy. Each array is rotated with respect to the layers above and below. In sensory bristles, chitin primarily accumulates in bands parallel to the proximal/distal axis of the bristle. These bands are visible by confocal microscopy providing experimental advantages. We have used this cell type and an edited chitin synthase gene to establish that the bands of chitin are closely associated with stripes of chitin synthase. This argues that the localization of chitin synthase plays an important role in mediating the patterned deposition of chitin in insect cuticle. However, other data suggest this connection may not be absolute. Several genes are essential for proper chitin deposition. We found one of these, *Rab11* is required for the insertion of chitin synthase into the plasma membrane and a second, *duskylike* is required for plasma membrane chitin synthase to properly localize into stripes. We also established that the actin cytoskeleton is required for the proper localization of chitin synthase and chitin in developing sensory bristles. An unexpected finding is that chitin synthase and other membrane proteins are shed during or after the process of cuticle deposition and this may explain cases where there is a lack of a sharp phenotypic boundary between cells that have or lack chitin synthase activity.

Introduction

Chitin is an abundant and widespread extracellular polymer found in many types of eukaryotic organisms from fungi to vertebrates. It is synthesized by the multi-pass transmembrane enzyme Chitin Synthase (CS). This enzyme has principally been studied in fungi and insects, where chitin plays important structural roles. In fungi chitin is a constituent of the cell wall and the number of CS genes is quite variable (Merzendorfer, 2011). For example, S. cereviase has 3 CS genes (Gohlke et al., 2017) while Aspergillius fumigatus has 8 (Muszkieta et al., 2014). Chitin in fungal cell walls is not uniformly distributed and in these systems different CS's appear to have different subcellular localizations and to mediate chitin synthesis in different parts of the cell wall including the bud ring (Cabib and Bowers, 1971; Foltman et al., 2018). In insects, chitin is a major component of the cuticular exoskeleton, the apical surface of trachea and the peritrophic membrane that lines the gut (Merzendorfer, 2011). In the cuticle, it is in parallel arrays while in the peritrophic membrane it is a fibrous mesh. There are two CS genes in insects, one functions in the formation of the cuticular exoskeleton and tracheal lining and the other synthesizes the chitin found in the peritrophic membrane (Merzendorfer, 2011). In Drosophila the chitin synthase enzyme required for the synthesis of cuticle chitin is encoded by the *kkv* gene (Moussian et al., 2005; Ostrowski et al., 2002). On the surface, the larger number of CS encoding genes in fungi is surprising as the insect exoskeleton is a morphologically more complicated and varied structure than the fungal cell wall.

The most conserved region in all chitin synthases is the catalytic domain (con1) (Dorfmueller et al., 2014; Nagahashi et al., 1995; Yabe et al., 1998) and this region is essential and sufficient for chitobiose synthesis by SC-CHS2. A second conserved region (con2-ref) is essential for the synthesis of long chito-oligosaccharide, and seems likely to be essential for the translocation of growing chitin chains (Dorfmueller et al., 2014; Yabe et al., 1998). Con1 from SC-CHS2 shows substantially higher sequence conservation than con2, but both can be recognized in insect chitin synthases such as Drosophila Kkv. Both of these regions are thought to be cytoplasmic in yeast CHS2, although there is evidence for two transmembrane domains separating the catalytic site from at least the c terminal most part of Con2 (Gohlke et al., 2017) . The insect cuticle CS is typically larger than most fungal CS proteins. For example, the Drosophila CS1 contains 1615 amino acids while yeast CHS3 contains 1165 amino acids. The larger size might allow the insect protein to interact with a larger number of other proteins and this could be important in the development of the morphological complexity of insect cuticle. All CS are multi-pass transmembrane proteins. The number of inferred transmembrane domains varies from ~5 to 18 with fungal CS proteins generally predicted to contain many fewer putative transmembrane domains than insect CS proteins (Gohlke et al., 2017; Merzendorfer, 2011) (Merzendorfer and Zimoch, 2003). However, since different programs predict different numbers of transmembrane domains for individual CS until direct experimental data provides answers there will be uncertainty (Gohlke et al., 2017). Indeed, in the case of fungal chitin synthases direct experimental data established that the computer programs for predicting transmembrane domains are useful but not able to accurately predict membrane protein topology (Gohlke et al., 2017). We report here experimental evidence that the amino terminus of Drosophila Kkv is in the cytoplasm and the carboxy terminus in the extracellular space.

The arrangement of chitin in insect cuticle may differ in different structures. Over most of the cuticle chitin is found in layers of parallel arrays of chitin fibrils with each layer rotated with respect to its neighbors above and below (Bouligand, 1972; Moussian, 2013; Moussian et al., 2006a). As assayed by confocal microscopy, in the cuticle that covers the shaft of sensory bristles chitin is most abundant in bands that run parallel to the proximal-distal axis of the bristle (Nagaraj and Adler, 2012). In transmission electron micrographs we did not see evidence for the presence of chitin layers in bristles or in hairs (trichomes), but whether this represents a true difference or is a consequence of a higher density of cuticle proteins masking the layers remains uncertain. In this paper we make use of the bristle shaft as a model cell type to study patterned chitin deposition in insects. The large size of these polypoid cells makes them favorable for this purpose.

The insect cuticle Chitin synthase has been particularly difficult to study in vitro and what is known about it and the process of chitin deposition is relatively limited (Merzendorfer, 2011). Chitin fibrils are insoluble at physiological pH (Elieh-Ali-Komi and Hamblin, 2016), which restricts models for how patterned chitin deposition can be mediated at the cellular level (Fig 1A). One possibility is that in insects as in fungi CS is localized in a patterned way to specific membrane domains and chitin deposition is directly patterned by this. In insect epidermal cells rows of elevated membrane called undulae have been proposed to be the site of chitin deposition (Moussian et al., 2007) (Moussian et al., 2006a). The tips of the undulae are associated with extracellular matrix (Moussian et al., 2006a) (Adler, 2017) but it is not clear if this material is composed of chitin, cuticle proteins, other extracellular proteins/carbohydrate or more than one of these. Interestingly, prominent undulae are not seen during the deposition of some chitin containing cuticle, for example the cuticle that covers wing hairs or bristles (Adler, 2017; Sobala and Adler, 2016). Thus, it seems unlikely that undulae per se are essential for chitin or cuticle deposition. An alternative model is that the synthesis of chitin is not patterned but that chitin binding proteins bind to chitin fibrils as they are extruded through the membrane and serve as carriers to mediate the movement of the chitin to the correct place in the developing cuticle. There are a large number of proteins encoded by insect genomes that contain a chitin binding domain and could be part of such a system (Karouzou et al., 2007; Willis, 2010) . In such a model, it seems likely that one or more unidentified proteins are first deposited in a patterned way and they interact with the chitin binding protein-chitin complex to guide the location for chitin fibril deposition. A third model is that CS containing exosomes/chitosomes are secreted and these are guided to the correct location for patterned chitin fibril deposition by interactions between exosome membrane proteins and one or more cuticle components. There are suggestions in support of this sort of model in the literature but evidence for exosomes has not been reported in transmission EM studies on cuticle deposition in Drosophila (e.g. (Sobala and Adler, 2016)). However, here we report evidence that Kkv (i.e. Drosophila CS) is shed during or after the synthesis of the pupal cuticle consistent with a possible exosome model. One difference between the three models is that the first predicts that *kkv* should act strictly cell autonomously while the second and third models suggest the possibility of limited cell non-autonomy. Previous experiments have described *kkv* as acting cell autonomously (Ren et al., 2005) (Adler et al., 2013) but we show here experimental evidence that argues for a small degree of non-autonomy.

As noted above the accumulation of chitin in the cuticle of Drosophila sensory bristles occurs primarily in bands parallel to the long axis of the bristle (Nagaraj and Adler, 2012) and we have used this to examine the relationship between the localization of Chitin Synthase (Kkv) to the patterned accumulation of chitin. We find Kkv is closely associated with these chitin bands during cuticle deposition. Notably, this is true even when both patterns are highly abnormal. The accumulation of Kkv is not smooth like the chitin bands but is punctate. To clarify the text we use stripes to describe the accumulation of Kkv and bands to describe chitin. We previously identified several genes whose function was essential for the accumulation of bristle chitin in parallel bands (Nagaraj and Adler, 2012). Knocking down the function of two of these genes resulted in a failure of the accumulation of Kkv in stripes. These observations link the patterning of extracellular chitin to the patterning of Kkv localization in the apical plasma membrane of epithelial cells and begin the identification of genes that mediate both the insertion of Kkv into the plasma membrane and the organization of Kkv in stripes along the proximal distal axis of the bristle.

We also observed that a putative catalytically inactive Kkv did not localize properly suggesting the possibility that the secretion of chitin is important for either the establishment or maintenance of Kkv localization. A second possibility is that the active site mutation altered the structure of the protein and that led to the abnormal localization.

Results

Generation and characterization of transgenes and edited genes that encode tagged Kkv.

As a first step in examining the role of CS localization in the patterning of chitin deposition we generated a series of new genetic reagents consisting of 4 different *UAS-kkv* transgenes and two edits of the endogenous *kkv* gene (Fig 1BC) (see Methods for details).

In one of the UAS transgenes the *kkv* open reading frame was tagged on the C terminus by the bright mNeonGreen (NG) fluorescent protein (Shaner et al., 2013) (*UAS-kkv::NG*). In a second it was tagged by the ollas epitope tag (Park et al., 2008) and his_6 (*UAS-kkv-OH*). We also examined a variant of the NG tagged protein that contained the amino acid change found in the amorphic *kkv*-1 allele (R896K) (Moussian et al., 2005). In the fourth, multiple changes were made to the catalytic domain to change convert it to a mosquito sequence. At most only quite modest gain of function phenotypes were observed when either of these transgenes were over expressed (see Supplementary Text File 1 and Fig S1). It is not surprising that our UAS transgenes do not show dramatic gain of function phenotypes as Moussian and colleagues (Moussian et al., 2015a) have established that Kkv requires a second protein (MH2 domain containing - either Reb or Exp) for the accumulation of chitin.

We used CRISPR/Cas9 and Homology Dependent Repair (HDR) to edit the endogenous *kkv* gene to add two different C terminal tails (see methods for details). In one we added the mNeonGreen fluorescent

protein (NG) (Shaner et al., 2013) while in the second we added *smFP-HA* (Viswanathan et al., 2015) (Fig 1BC), which is a variant of super folder GFP with multiple HA tags inserted into loops of GFP. Both *kkv::NG* and *kkv::smFP-HA* were homozygous viable and showed no mutant phenotypes under a stereo microscope. Homozygous *kkv::NG* flies also showed no morphological defects when we examined mounted cuticle by compound light microscopy or scanning electron microscopy (Fig 2EF, S2CD). This was also true for *kkv::NG/DF* and *kkv::NG/kkv*^{1}. The data establish the edited gene and protein are close to if not functionally equivalent to wild type. When we examined *kkv::smFP-HA* cuticle by SEM or compound light microscopy we detected a mutant phenotype in wing hairs consisting primarily of thin and bent hairs (Figs 2EF, S2A). The phenotype appeared slightly stronger in *kkv::smFP-HA*/*Df* flies but we did not attempt to quantify this (Fig S2AB). In *ap-Gal4; UAS-kkv::NG kkv::smFP-HA/kkv::smGFP-HA* and *ap-Gal4; UAS-kkv::NG kkv::smFP-HA/Df(3R)ED5156* flies the wing hair phenotype was rescued in the dorsal wing cells where *ap* drives expression of *kkv::NG* but not in the ventral wing cells that served as an internal control (Fig 2GH). Similar results were obtained when *UAS-kkv-OH* was substituted for *UAS-kkv::NG.* We examined pupae that expressed Kkv::NG and Kkv::smFP-HA by in vivo confocal imaging. The level of fluorescence was much higher for Kkv::NG (we estimate it as being ~15X brighter (see Methods and Fig S3)) and hence we used it for all of the protein localization experiments described below. These data are consistent with *kkv::smFP-HA* being a viable hypomorphic allele of *kkv* where a lower than normal level of protein accumulates. The hair phenotype is likely due to this structure requiring a higher level of chitin for normal morphogenesis.

Subcellular Localization of Kkv

We first used the *UAS* transgenes to examine the subcellular localization of Kkv. Kkv::NG localized on the apical surface of the large polytene salivary gland cells of *ptc>kkv::NG* larvae (Fig S4I). The large size of these cells makes them favorable for detecting the apical localization. In wing discs of *ptc>kkv::NG* larvae we observed the expected stripe of expression (Fig S5A) in the middle of the wing. We did not see any evidence for the secretion of Kkv::NG in these experiments. As an internal positive control, the larvae also expressed a secreted ChtVis-tdTomato chitin reporter (in red) (Sobala et al., 2015). As expected, Cht-Vis could be detected in the extracellular space between the disc epithelium and peripodial membrane cells. The stripe of Kkv::NG was obvious in living wing discs and in fixed wing discs stained with anti-NG antibodies, establishing that these antibodies did not cross-react with endogenous proteins in wing cells. As is elaborated later, similar specificity was observed for *ptc>kkv::OH* using an anti-ollas monoclonal antibody and when we used a rabbit polyclonal antibody (*anti-Kkv-M*) made against a region from the central part of the Kkv protein (aa1097-1246) to stain the stripe of *Kkv::NG* expression in wing discs. In Z sections we observed that Kkv::NG was preferentially localized to the apical surface of the wing disc cells (Fig S5B, arrow), as expected for a protein involved in the synthesis of a cuticle component and is consistent on observations of others in different contexts (Maue et al., 2009; Moussian et al., 2015; Zimoch and Merzendorfer, 2002). We also examined fixed *ap>kkv::NG* pupal wings where F-actin was stained with Alexa 568 phalloidin and Kkv-NG by anti-NG antibody (Fig 4G-L). As expected for a transmembrane protein Kkv::NG was localized external to the actin filaments found in the center of growing hairs (Fig 3G-I) (Adler et al., 2013; Turner and Adler, 1998; Wong and

Adler, 1993). This close localization is reminiscent of the apical F-actin and chitin in wing hairs (Adler et al., 2013) and in late stages of trachea development in Drosophila embryos (Ozturk-Colak et al., 2016). At this stage when cell flattening and wing expansion is under way, a large disc of F-actin is seen under each hair (Fig 3K) (Adler et al., 2013). We did not observe a similar disc of Kkv::NG in such wings (Fig 4J). Thus, we conclude there is not a universal connection between the localization of sub membranous F-actin and Kkv in the juxtaposed membrane (Fig 3K).

When expressed in developing bristles by *neur-Gal4*, Kkv::NG accumulated in a manner similar to, albeit perhaps a bit less precisely than that seen for the protein encoded by the edited endogenous gene (see Fig 4ABDG). Most of our localization experiments used the edited endogenous gene to eliminate potential over expression issues. However, for some experiments that required immunostaining the use of the UAS transgenes was valuable as it allowed us to examine younger animals where cuticle deposition had not made immunostaining problematic.

The use of the Neon Green (and Ollas-His_6) tag to localize Kkv requires that the tag remains associated with the enzyme to provide a meaningful localization. Since chitin synthases are often cleaved and in some cases this has been linked to enzyme activation (Broehan et al., 2007; Merzendorfer and Zimoch, 2003) (Zhang and Zhu, 2013) this is a concern (we have also seen evidence for cleavage of Kkv on Western blots - pna, preliminary results). To test if the tags remained associated with the enzyme we stained pupae where *UAS-kkv::NG* expression was driven by *neur-Gal4* using both a commercially available anti-NG monoclonal and our anti-Kkv-M rabbit polyclonal antibody. We observed a clear co-localization in stripes of puncta along the proximal distal axis in bristles using the two antibodies (Fig 4 DEF). This establishes that the neon green tag from the fusion protein is an accurate reporter for the Kkv protein. We also carried out similar co-localization experiments on *neur>kkv::OH* pupae and observed a similar co-localization using anti-Ollas and anti-Kkv antibodies (Fig 4 GHI). We found similar results for the accumulation of Kkv::NG in pupal wings and wing hairs when expression was driven by *ap-Gal4* (Fig 4MNO).

Localization of Kkv encoded by the edited endogenous gene:

We first examined the accumulation of Kkv::NG from the edited endogenous gene in pupal wings as this tissue is the best characterized for the timing of cuticle deposition and gene expression (Adler et al., 2013; Sobala and Adler, 2016). Previously we found that we could first detect chitin in pupal wings in developing hairs around 42 hr after white prepupae (awp) (Adler et al., 2013). We observed Kkv::NG in developing hairs in living pupal wings at 42, 49 and 58 hrs awp (after white pupae) (Fig 3C). The level of fluorescence was lower in 42 hr hairs than in 49 hr hairs. We could also detect Kkv::NG fluorescence in the apical surface of wing cells with higher levels at cell boundaries. This was a bit surprising since the procuticle is not being made and we have not detected chitin in the wing blade at this time (Adler et al., 2013; Sobala and Adler, 2016). We also examined pupal wings that were younger than 40 hrs awp. Confocal images of such wings did not show any fluorescence when examined under the same conditions as >40 hr wings (Fig 3A). However, in digitally enhanced images we detected the

accumulation of Kkv::Ng in what is likely the proximal part of the hair (Fig 3B). In older wings (e.g. 76 hr) during the middle of procuticle deposition the apical membrane fluorescence was stronger than at earlier times and we could see the pedestals that the hairs are found on at late stages (Fig 3F) (Sobala and Adler, 2016). As noted above, similar, albeit a bit messier results were obtained when we examined *ap>kkv::NG* pupal wings.

We next examined the localization of Kkv::NG in thoracic bristles by in vivo imaging from ~40-80 hr awp. Previously we found that chitin accumulated in bands along the proximal distal axis of thoracic bristles starting around 42 hr awp (Nagaraj and Adler, 2012). The level of Kkv::NG fluorescence in younger than 50hr awp bristles was lower than in older bristles. (Fig S6). At both early and later stages, Kkv::NG fluorescence had a punctate appearance within an overall pattern of stripes along the proximal distal axis of the bristle (Figs 4A-C, 5J, S5E, S6). In some samples, we observed what appeared to be a pair of relatively closely situated stripes. As development proceeded, the stripes became more complete although they never reached the completeness and smoothness seen with chitin bands. In older animals (>70 hrs) the pattern became somewhat less distinct with more inter-stripe fluorescence (Fig S6. When we examined orthogonal views of bristle image stacks the stripes of Kkv were obvious (Fig 5N). Unless stated otherwise, in subsequent in vivo imaging experiments, we primarily examined bristles from 50-65 hr old animals as these showed the most dramatic “stripe pattern”. Control experiments with Oregon-R pupae established that the florescence we were observing was due to the edited *kkv* gene and not to autofluorescence (Fig S5C-F).

As noted in the introduction the relationship between the patterned deposition of chitin and the localization of CS in insects is not clear. To investigate this we carried out experiments where we localized both Kkv::NG and our chitin reporter (Cht-Vis) in bristles in living pupae (Sobala et al., 2015). The bands of ChtVis differed from those of Kkv::NG by being smooth rather than punctate (Fig 4C-C’’). However, the two patterns were largely co-aligned in stripes along the proximal distal axis of bristles. In cross section the ChtVis signal was usually exterior to the Kkv-NG signal as expected for chitin being secreted and CS being a transmembrane protein localized to the apical plasma membrane (Fig 5O). The stripe of Kkv::NG was often also offset a bit from the ChtVis signal, which could be a consequence of ChtVis reporting on chitin (an accumulated product) while the Kkv::NG signal represent protein at a particular instance in time. The different cellular location (plasma membrane vs extracellular) and geometry likely contributes to this (Fig S7).

The actin cytoskeleton influences the accumulation of Kkv

In several experiments, we explored the relationship between Kkv::NG accumulation and the large bundles of cross-linked F-actin found in bristles (Tilney et al., 1995). These experiments were complicated by the breakdown of the actin bundles, which starts around 43 hr (Guild et al., 2002), and our inability to reliably immunostain bristles older than about 48 hr awp. In our best experiments we examined pupae that were 48hr or younger. An additional complication is geometric and due to Kkv being in the plasma membrane (and the NG in Kkv::NG being extracellular as described below) while the

F-actin extends some distance into the cytoplasm (Tilney et al., 1995) (Fig S7). Using an F-actin reporter (Lifeact-Ruby - (Hatan et al., 2011; Riedl et al., 2008) we observed a close connection between the localization of Kkv::NG and the large bundles of F-actin in *neur>lifeact-Ruby; kkv::NG* pupae. The results varied from the two appearing to co-localize to their being slightly offset (Fig 5H-J, H'-J') consistent with the geometry considerations (Fig S7).

The large bundles of highly cross-linked actin filaments support the shape of growing bristles and in their absence in sn^3 f^{36} double mutants the resulting bristles are bent, curved, split, shorter and stand more upright than normal (Guild et al., 2002; Tilney et al., 2004; Tilney et al., 1995). In separate experiments, we observed an abnormal distribution of chitin and Kkv::NG in living sn^3 f^{36} double mutants. The robust parallel array of chitin bands and Kkv::NG stripes were severely disrupted (Fig 5AB). Kkv::NG was primarily in the plasma membrane and the chitin appeared to be extracellular so the bundles of F-actin do not appear to be required for the targeting of Kkv to the plasma membrane or for the secretion of either chitin or the chitin reporter. To determine the relationship between the abnormal stripes of Kkv::NG and chitin we examined the distribution of both in the same living bristle. We found the linkage between chitin and Kkv::NG was maintained even in these highly abnormal bristles (Fig 5CDE). We often observed stripes of Kkv::NG on both sides of a band of chitin. We have seen this in normal bristles but by casual observation less frequently.

Proteins required for the proper localization of Kkv.

We previously established that Rab11 and exocyst function is required for the deposition of cuticle and the bands of chitin in bristles (Nagaraj and Adler, 2012). Affected bristles become unstable and collapse after the highly cross linked F-actin bundles in developing bristles begin to depolymerize (Guild et al., 2002; Nagaraj and Adler, 2012). To determine if the failure to form chitin bands was associated with a failure to properly localize CS we examined Kkv::NG in thoracic bristles of living *neur-Gal4 Gal80-ts/Rab11 RNAi; kkv-NG/kkv-NG* pupae that were shifted to 29.5°C at wpp (white prepupae). When allowed to develop to adulthood these animals showed the extreme stub macrocheatae phenotype described previously (Nagaraj and Adler, 2012). The morphology of the bristles was dependent on pupal age. In the youngest animals examined, the bristles were beginning to show the blebbing characteristic of the early stages of the collapse program (Nagaraj and Adler, 2012). In older animals the collapsed stub bristle morphology was seen (Fig 5G, arrow). The stripes of Kkv::NG were lost and in Z sections we found that the protein was not preferentially localized to the plasma membrane and instead was found in the cytoplasm (Fig 5P). These observations indicate that Rab11 function is required for the proper trafficking of Kkv to the plasma membrane and this can explain the loss of chitin bands in the Rab11 mutant (Nagaraj and Adler, 2012).

The Zona Pellucida domain containing Dusky-Like (Dyl) protein acts as a Rab-11 effector for chitin deposition in bristles (Nagaraj and Adler, 2012). To determine if Dyl was required for the proper localization of Kkv we examined Kkv::NG in thoracic bristles of living *UAS-dyl-RNAi/+; neur-Gal4 kkv::NG/kkv::Ng* pupae where Dyl expression was knocked down. The bristle collapse phenotype seen

in these bristles is similar that of the Rab11 knock down; albeit slightly weaker as not all macrocheatae show the extreme stub phenotype. We observed these bristles in the blebbing stage and observed the loss of the robust striping pattern of Kkv::NG accumulation (Fig 5F). Kkv::NG in such bristles was primarily seen spread around the plasma membrane (Fig 5Q). The distribution was not uniform but was far from the nicely spaced stripes seen in wild type. The data argue that Dyl is required for the localization of Kkv::NG in stripes but not for its insertion into the plasma membrane. The difference in Kkv::NG localization between the Rab11 and Dyl knockdowns suggests that these two genes and proteins mediate different steps in the localization of Kkv.

To complement these experiments we also simultaneously localized Kkv-NG and Dyl in bristles by immunostaining. The stripes of Kkv::NG and Dyl were interdigitated but did not appear to touch (Fig 5KLM). As described above and elsewhere (Nagaraj and Adler, 2012) the function of the actin cytoskeleton, Rab11 and *dyl* are required for the normal accumulation of both chitin and Kkv::NG in developing bristles. To determine if the function of the actin cytoskeleton is required for the normal subcellular localization of Dyl in stripes we immunolocalized Dyl in developing sn^3 f^{36} bristles. We found that the normal striped accumulation of Dyl was disrupted in the sn^3 f^{36} bristles (Fig S8AB).

Localization of an inactive mutant Kkv

We next addressed the question of whether the catalytic activity of Kkv might impact its subcellular localization by placing a R896K mutation put into *UAS-kkv::NG*. This missense mutation is the cause of the amorphic kkv^1 allele and is in an invariant site that is part of the enzyme's active site (Dorfmueller et al., 2014; Merzendorfer, 2006; Moussian et al., 2005; Nagahashi et al., 1995). We first tested if this transgene could rescue the wing hair phenotype seen in *kkv::*smFP flies. The wings of *ap-Gal4/+; UAS-kkv-R896K::NG kkv::smFP/kkv::smFP* flies showed no evidence of rescue of the *kkv::smFP* hair phenotype (Fig 2IJ). The failure of this transgene, which encodes a protein that very likely has little or no catalytic activity, provides support for the validity of the *kkv::smFP* rescue assay.

When expressed by *ptc-Gal4* Kkv::NG preferentially localizes to the apical surface of salivary gland cells (Fig S4I), while in comparison Kkv R896K::NG was distributed relatively evenly in the cytoplasm (Fig S4J). At higher magnification we observed Kkv::NG accumulated in what appear to be vesicles (Fig S4I') (The salivary gland cells are packed full of vesicles at this stage). In addition to outline fluorescence we observed puncta of Neon Green fluorescence on the vesicles (Fig S4I', arrow). The mutant protein accumulation appeared different with accumulation either between vesicles or in abnormally shaped vesicles (Fig S4 J'). As noted earlier, Kkv::NG accumulates in wing hairs (Fig 3C-L, S4A) the most apical part of wing epidermal cells. In contrast, Kkv R896K::NG did not accumulate in the hair. Rather, it accumulated relatively evenly in the cytoplasm (it appears to be restricted from the nucleus)) (Fig S4B). This was not due to delayed hair development as when we stained for F-actin using phalloidin we observed the expected hairs with Kkv R896K::NG in the cytoplasm (Fig 4PQR, Fig S4CD). In developing bristles Kkv R896K::NG did not routinely accumulate in proximal/distal stripes as the wild type protein does. Rather, much of the protein was not found on the plasma membrane and there were uneven

regions with varying levels of fluorescence (Fig S4E-H). One possibility for the mislocalization is that the mutant protein might be cleaved so that NG was no longer a valid reporter for the enzyme. To test this we immunostained both pupal wings and bristles using both the anti-NG and anti-Kkv-M antibodies. Extensive co-localization of the two staining signals indicated that the NG tag remained a valid reporter for the R896K mutant (Fig 4JKL, PQR).

A Kkv with a catalytic domain mutated to a mosquito catalytic domain is functional.

We next attempted a more ambitious test of the *kkv-smFP* rescue assay using a UAS transgene where the con1 domain of *kkv* was replaced by the equivalent region of a mosquito chitin synthase (*UAS-kkv-mos::NG* – see Fig 1B and Methods for details). We generated *ap-GaL4/+; UAS-kkv-mos::NG kkv::smFP/kkv::smFP* flies and found that the mutant wing hair phenotype of *kkv::smFP* to be fully rescued in the dorsal but not ventral wing surface hairs (Fig 2KL) indicating that this "hybrid" protein is active.

Topology of Kkv

Different programs that predict transmembrane domains give different predictions for the topology of Kkv (see Methods for more information). The predictions differ in terms of the number of transmembrane domains and in the predicted location (cytoplasmic vs extracellular) of different protein regions. For example, the TMPRED program predicts 18 transmembrane domains (TMDs) while TMHMM2.0 predicts 15 TMDs. Among 14 different predictions a set of 14 putative TMDs were included in 13 or 14 predictions. Fig 6B shows the locations of these "consensus predictions". The reagents we generated for other reasons provided us with tools we could use to probe the topology of Kkv. We immunostained *ptc>kkv-OH* (and *ptc>kkv-NG*) wing discs either with or without permeabilization of the plasma membrane with Triton X-100 (Fig 6A). We found both anti-NG and anti-Ollas antibodies stained wing discs in the absence of permeabilization indicating that the C terminus is exposed to the extracellular space (Fig 6A). All of the topology programs predicted this. In contrast when we used an anti-Kkv polyclonal antibody (anti-Kkv-M) raised against aa 1097-1246 we did not see any staining in the absence of Triton X-100 permeablization (Fig 6A), arguing this region is intracellular. This disagrees with the consensus prediction. Similar results were obtained when we used antibodies directed against aa 53-66 and also antibodies directed against aa 530-541 – a region located not far from the catalytic domain (Fig 6AB). These results indicate that these regions of Kkv are also located in the cytoplasm. It is worth noting that no programs predicted a transmembrane domain in the region encompassing aa 1-53, which when combined with our data suggests that the amino terminus of Kkv is located in the cytoplasm. None of the programs predicted a transmembrane domain between the aa 530 and the catalytic domain suggesting this region is part of the same cytoplasmic loop. Our experimental data does not agree with the consensus TMD predictions as they suggest that the region between 1097-1246 is extracellular but an antibody directed against this region was unable to stain the protein in the

absence of Triton X-100 treatment. No differences were seen when we ran several of the computer analyses with the alternative Kkv isoform.

Kkv is shed

In experiments where we imaged Kkv::NG in living pupae we noticed fluorescent puncta in the extracellular space between the pupal cuticle and the epidermal cells that were in the process of synthesizing the adult cuticle (Fig 4B, S3A, Fig S9A). To investigate this in more detail we obtained large Z stacks that extended from the pupal cuticle to below the apical surface of the epidermal cells. Pupal cuticle in 50 hr pupae shows substantial autoflourescence so we examined and compared *Ore-R* and *kkv::NG* pupae to determine what if any fluorescence was due to the presence of the Kkv-NG protein. The autofluorescence of the thoracic pupal cuticle of Ore-R was spatially relatively even (Fig 7D). In contrast, the fluorescence of pupal cuticle of kkv-NG flies was much more uneven with both puncta (arrow) and lines (arrowhead) of bright fluorescence (Fig 7A). No fluorescence was observed in the region between the pupal cuticle and the apical surface of the epithelial cells in Ore-R pupae (Fig 7E). In contrast, in this region many fluorescent puncta were observed in *kkv::NG* pupae (Fig 7BC)(arrow). A majority of these were located close to the pupal cuticle but some were observed throughout the region. Most of the *puncta located close to the pupal* cuticle were stable but many of those located lower were mobile (movie S1). Since the fluorescent puncta were only seen when the *kkv::NG* gene was present we interpret the puncta as evidence of shed Kkv::NG. Since the puncta were located above the impermeable adult cuticle (which is in the process of being synthesized), it seems likely that the Kkv::NG was shed during or after the synthesis of the pupal cuticle and before the synthesis of the adult cuticle began. Consistent with this hypothesis we observed puncta in 28hr pupae, well before the start of adult cuticle deposition (Sobala and Adler, 2016). We also observed puncta in very young pupae (20 hr awp) prior to the detachment of the epithelial cells from the pupal cuticle (Fig. S9B). We observed similar puncta when we examined *ap>kkv::NG* pupae (Fig S9C) but not from *ap>kkv-R896K*::NG pupae (Fig S9D), arguing that to be shed Kkv needs to be localized apically.

The highest concentration of puncta were over the dorsal thoracic midline (Fig S9AB). There were also a large number of puncta over the dorsal abdomen and they were seen at a lower frequency in the wing, legs and head. In the abdomen the puncta tended to align parallel to the segment boundary (Fig S3A arrows).

All of the experiments where we detected puncta in living pupae required imaging of the Kkv::NG fusion protein. Experiments described earlier established that NG was a valid reporter for Kkv in bristles so it seemed likely that it was also a valid reporter for Kkv in puncta. In an attempt to test if this was correct we immunostained pupal cuticle using both anti-NG and anti-Kkv-M antibodies. Among the puncta detected 69.7% stained with both antibodies indicating most puncta contained both NG and Kkv (Fig S10, arrows).

The shedding of Kkv::NG could be specific for Kkv or it could reflect a process that leads to the shedding of many if not all of the proteins located in the apical plasma membrane. To distinguish between these

possibilities we examined live *ap-Gal4/+; UAS-mCD8-GFP*/+ pupae. These animals showed a large number of fluorescent puncta present in the space between the pupal cuticle and the apical surface of the epithelial cells (Fig 7GHI). As was the case for the puncta in *kkv::NG* pupae many of the puncta were mobile (movie S2). We conclude that the shedding of membrane proteins is not specific for Kkv or proteins involved in cuticle deposition.

Cell autonomy of *kkv*

We previously observed clones of *kkv* in the wing where they lead to faint and flaccid wing hairs (Ren et al., 2005). By examining the morphology of the hairs, the clones appeared to be completely cell autonomous. However, in adult wings the hair is located over the center of the cell and it is not clear if we could detect limited partial cell non-autonomy in such an assay. Given the close juxtaposition of the epidermal cells and the cuticle during cuticle deposition it seems unlikely that CS containing vesicles, if they exist, could diffuse far. To determine if we could detect any evidence of non-autonomy for *kkv* we needed an assay that allowed us to identify *kkv* clones and examine them at a higher resolution than is possible in the light microscope. We found that we could fracture adult cuticle and by scanning electron microscopy (SEM) detect a layered structure. The layers were very distinctive in abdominal cuticle (Fig S2G) consistent with the robust layering in abdominal procuticle seen by TEM (Fig S2H). We also examined wings attached to studs in a vertical position, fractured and imaged by SEM. In wing cuticle we could also detect a layered structure that presumably reflects the banding of chitin in the procuticle (Fig 8C). The layering was less distinctive than in the abdominal cuticle, which we also found to be true by TEM (Sobala and Adler, 2016). We next fractured and observed wings carrying *kkv* loss of function clones. We were able to identify mutant clones by the presence of the *kkv* flaccid hair phenotype (Fig 8BDE, arrows) (Ren et al., 2005). If there was complete cell autonomy we predicted a sharp change in wing cuticle thickness at wt-mutant clone boundaries (Fig 8A). In contrast, if there was a small degree of cell non-autonomy we predicted that we would see a smooth change in cuticle thickness near the edge of clones (Fig 8A). In all of the clones (n=9) we examined there was a smooth transition in cuticle thickness (Fig 8DE). This transition zone appeared to be restricted to a mutant cell and its direct neighbor.

Discussion:

The patterning of Chitin deposition is linked to the localization of Kkv

Our observations generally support a model where the localization of chitin deposition is closely linked to the localization of Kkv (Chitin synthase). The most compelling data being that the localization of chitin and Kkv remain linked even when the distribution of both is abnormal. A limitation of our

observations is that they focused on the bands of chitin seen along the proximal distal axis of developing sensory bristles. The cuticle that covers the sensory bristles differs in two ways from the cuticle that covers much of the fly's body. First, we have not detected the layering of chitin in TEM studies of bristles although this could simply be due to a higher concentration other components in the procuticle interfering with our ability to detect the layering. A second difference is that the prominent undulae seen in most cells synthesizing cuticle were not detected in bristle forming cells (Adler, 2017). Further studies will be needed to determine if the close connection between chitin and chitin synthase is a general result for arthropod epithelial cells, but that seems likely. The close connection between CS and chitin is similar to that seen in yeast and fungi (Leal-Morales et al., 1994) (Chuang and Schekman, 1996) (Santos and Snyder, 1997) (Kozubowski et al., 2003) (Latge et al., 2005) and is reminiscent of the connection between cellulose and cellulose synthase in plants (Polko and Kieber, 2019).

Our SEM analysis of *kkv* mutant clones showed that there was a gradual thinning of the procuticle in the region where mutant and wild type cells were juxtaposed. That result and our other results showing Kkv and chitin are closely localized to one another is compatible with models where at least some localized Kkv becomes incorporated into secreted vesicles, which have some but limited ability to move in the extracellular space between cuticle and the apical plasma membrane. It is also compatible with models where localized Kkv secretes chitin fibers that can bind a carrier protein to form a complex that has a limited ability to move prior to deposition. It does not fit well with models where localized Kkv always leads to chitin fiber deposition close to the site of synthesis. An alternative possibility is that the SEM assay is misleading. For example, the gradual change in cuticle thickness detected by SEM might not be directly related to a different amount of chitin fibrils, but rather mechanical forces that are part of wing maturation lead to a smooth transition between the cuticle above neighboring mutant and wild type cells independent of chitin content.

The localization of Kkv in bristles requires both the intracellular transport of the protein into the plasma membrane and its restriction to stripes. In principle, one or two (or more) genetic pathways could mediate these steps. We previously identified the *Rab11* and *dyl* as being essential for the normal deposition of chitin in bands in bristles (Nagaraj and Adler, 2012). We found here that in the absence of *Rab11* function Kkv::NG failed to localize to the plasma membrane. In contrast, in the absence of *dyl* function Kkv::NG localized to the plasma membrane but it did not preferentially accumulate into the appropriate stripes. These results argue that there are at least two separate genetic pathways/functional systems that are essential for the localization of Chitin Synthase in insects. Rab11 is also required for the insertion of Dyl into the plasma membrane of developing bristles (Nagaraj and Adler, 2012) and we suspect it has a general role in either the intracellular transport of membrane proteins from the cell body to the shaft of the bristle and/or for insertion of proteins into the shaft plasma membrane. The role of *dyl* is of particular interest. Dyl is a ZP (zona pellucida) domain protein and like other ZP domain proteins it can polymerize (Jovine et al., 2005; Adler et al., 2013; Jovine et al., 2002) and it is thought that through this it can organize the apical extracellular matrix (Chanut-Delalande et al., 2012; Fernandes et al., 2010). The expression of *dyl* is almost entirely restricted to the period of envelop deposition (Sobala and Adler, 2016) and it accumulates in bands along the proximal distal axis of developing bristles (Nagaraj and Adler, 2012). Hence, it localizes in a way that is

519 appropriate for instructing the later accumulation of Kkv in stripes. We observed that the stripes of
520 Kkv::NG and Dyl were interdigitated and did not overlap. I suggest that that Dyl functions as a negative
521 factor to prevent the accumulation of Kkv::NG from regions of the bristle plasma membrane, but likely
522 does so indirectly as there appears to be space between the interdigitated bands. Future studies will be
523 needed to elucidate the mechanisms involved here (e.g. local Dyl could recruit a factor that removes
524 Kkv::NG from nearby regions of the membrane). In addition to Rab11 and Dyl we also established that
525 the large bundles of cross linked F-actin in bristles were also required for the normal deposition of chitin
526 bands. The localization of both Dyl and Kkv::NG were altered in developing *sn f* bristles. The
527 mislocalization of Dyl provides a mechanism for the mislocalization of Kkv::NG and the subsequent
528 abnormal chitin deposition in these bristles. A number of other genes have been identified that are
529 required for normal chitin deposition or where a loss of function leads to a *kkv* like wing hair phenotype
530 (Adler et al., 2013; Chaudhari et al., 2011; Moussian et al., 2015; Moussian et al., 2006b). It will be
531 interesting to determine if any of these also mediate Kkv localization.
532

533 It is possible that Kkv is actively cycled from the plasma membrane to cytoplasmic
534 endosomes/chitosomes and then back to the plasma membrane. There is strong evidence for the
535 recycling of chin synthase in yeast (Hernandez-Gonzalez et al., 2018; Knafler et al., 2019; Sacristan et al.,
536 2013) and Rab11 is a well-established marker for late endosomes (Calero-Cuenca and Sotillos, 2018)
537 (Welz et al., 2014) and the recycling of membrane proteins. In such a model the failure of Kkv::NG
538 localization in Rab11 deficient bristles could be due to a defect in recycling and not in the original
539 localization. This might also explain the failure of the presumptive catalytic defective Kkv-R896K mutant
540 protein to localize to the plasma membrane. It is possible that the inactive protein is more rapidly
541 removed from the membrane and that it is preferentially not recycled back to the plasma membrane or
542 recycled more slowly. This could be a quality control mechanism in the formation of insect cuticle.

543

544 ***kkv::smGFP* is useful as a system for structure function studies on CS.**

545 The importance of chitin synthase function for insects is demonstrated by the lethality associated even
546 with relatively small clones of *kkv* mutant cells (Ren et al., 2005) (Adler et al., 2013) and knocking down
547 *kkv* function for a restricted period of time in a limited set of epidermal cells (pna - unpublished). The
548 edited *kkv::smFP* allele is the only homozygous viable hypomorpic allele of *kkv* that we are aware of. As
549 we demonstrated the rescue of the wing hair phenotype of *kkv::smFP* is an easy assay for testing the
550 functionality of mutant Kkv proteins. This assay relies on UAS-Gal4 driven expression and this could be
551 misleading as overexpression could prevent distinguishing between mutants with reduced vs completely
552 normal activity. There are however, advantages to this assay compared to editing the endogenous
553 gene. It is important to consider that while CRISPR/Cas9 mediated editing is not difficult it still involves
554 more time and labor than UAS transgenesis and mutations identified as interesting by the UAS-Gal4
555 system can later be assessed using CRISPR/Cas9 to test for reduced but still significant chitin synthase
556 activity. Further, chitin synthases are known to function as multimers (Merzendorfer, 2011) (Gohlke et
557 al., 2017) and some mutations might be dominant negatives. These could be identified using the UAS-

Gal4 system but they would likely fail to be recovered by CRISPR/CAS9 mediated editing (or by classical mutagenesis) as they are likely to be dominant lethals. The UAS/Gal4 system could also be used to identify parts of the Kkv protein that are essential for its localization. The rescue by the Kkv-mos::NG protein shows the ability of this system to establish that a "mutant" Kkv can retain activity.

It was not surprising that the *kkv R896K* mutant showed no rescue activity as this missense mutation is considered an amorphic allele in Drosohila (Moussian et al., 2005) and a similar substitution in yeast contained only about 1% of wild type activity (Nagahashi et al., 1995). The failure of Kkv R896K to show rescue activity validates this system for structure function studies on the fly CS. It was surprising that this mutant protein did not localize properly. It is possible that the active site missense mutation disrupts both catalytic activity and normal protein folding and the folding defect leads to a failure to traffic the protein to the apical plasma membrane. As noted above it is also possible that the defect is not in the initial trafficking but is due to the inactive protein being recycled more quickly. Further studies will be required to distinguish between these hypotheses.

The *kkv::NG* and *kkv-smFP* edits were in the same location in the genome so it is likely that the greater activity and fluorescence of the *kkv::NG* edit compared to the *kkv-smFP* edit is not due to differences in transcription. Rather, our data suggests the smFP tagged only accumulates to a much lower level than the NG tagged protein. This could be due to a reduced half-life of the smFP tagged protein or to it folding less efficiently. One possible cause of this is the presence of multiple copies of the HA epitope tag in smFP. A study in yeast reported that a 3XHA tag could cause a dramatic decrease in the accumulation of some of the tagged proteins (Saiz-Baggetto et al., 2017). It is possible that a similar phenomenon can explain our results with *kkv-smFP*.

Significance of Kkv shedding?

The shedding of membrane proteins is not a rare phenomenon (e.g.(Lichtenthaler et al., 2018; van Niel et al., 2018)). In most cases the shed material is an ectodomain that is released due to proteolysis (Lichtenthaler et al., 2018). Such a shedding mechanism could explain the shedding of the NeonGreen component; however, it cannot explain our observation that most puncta stained with both an anti-NG antibody and an antibody directed against an internal and cytoplasmic region of Kkv. Hence, we suggest that the principle mechanism leading to the shed material is the shedding of a vesicle that contains much if not all of Kkv::NG (van Niel et al., 2018).

Our in vivo imaging of Kkv::NG provided evidence that Kkv::NG shedding occurs during or after the synthesis of the pupal cuticle. Our ability to detect the shedding was facilitated by the release of the pupal cuticle from the epidermal cells that secrete it. This does not happen with the synthesis of the adult (or larval cuticle) so we were not able to determine if Kkv::NG shedding also happens during the synthesis of the adult cuticle. It is unclear if the shedding is directly related to chitin synthase function (e.g. secreted chitosomes) or if it a consequence of a process that is not directly related to chitin deposition. We did not see evidence of shed puncta when Kkv R896K::NG was expressed in wing cells but that could simply be due to the protein not being localized to the apical surface and unrelated to it

being catalytically inactive. Our finding that mCD8-GFP is also shed suggests shedding is a general property of membrane proteins either during or after pupal cuticle deposition is complete. It is unclear what if any functional significance is connected to the shedding.

Kkv is present in the plasma membrane prior to procuticle formation.

Previous studies on the transcriptome of pupal wing cells (Ren et al., 2005; Sobala and Adler, 2016) established that *kkv* RNA was present prior to the start of wing blade procuticle deposition. Part of the reason for this is that wing hair chitin is deposited earlier than wing blade chitin. However, this cannot explain the presence of *kkv* RNA 8 hrs prior to the start of hair morphogenesis and 16 hrs prior to the earliest time we can detect hair chitin (Ren et al., 2005) nor the presence of Kkv protein in the general apical membrane (i.e. not in the hair) more than 12 hrs prior to blade procuticle deposition. These observations suggest the possibility that Kkv has an earlier function in cuticle formation that is not due directly to chitin synthesis (e.g. a structural role for the protein) or that the synthesis of unstable chitin could be important prior to the time when it begins to accumulate. Both of these hypotheses suggest it might be possible to detect abnormalities at early stages of cuticle formation in *kkv* mutant cells. It is worth noting that previously we detected several patches of extracellular chitin fibers on the apical surface of 29 hr awp pupal wings (Sobala et al., 2015). This is 11 hrs prior to when we first detect chitin in hairs (Adler et al., 2013) and 3 hours prior to the start of hair outgrowth (Wong and Adler, 1993).

Similarities and differences in bristle and tracheal chitin deposition.

Chitin deposition in bristles and the adult cuticle shows both similarities and differences from that described in trachea. In trachea the distribution of chitin changes during development. Starting out as a thick filament that largely fills the lumen it transforms into a thin zig zag shaped filament. The thin filament is eventually lost and during the this period chitin becomes concentrated over the distinctive tracheal taenidial folds (Devine et al., 2005; Ozturk-Colak et al., 2016; Tonning et al., 2005). It is not clear whether there is a complete loss of the chitin fibrils found in the central filament or if there is a reorganization of those fibrils into the taenidial fold chitin. In both tissues the disruption of the actin cytoskeleton results in an abnormal pattern of chitin; however in tracheal development a lack of chitin lead to an abnormal actin cytoskeleton while we did not see that in wing cells that lacked Kkv (Adler et al., 2013). In trachea Kkv puncta were seen more frequently over the taenidial folds than in the inter-fold region (Ozturk-Colak et al., 2016) but the patterning was much less distinctive than we have seen in bristles. Some of the differences between these results could be due to the use of UAS-Gal4 to drive the expression of Kkv in trachea as in our hands using this system resulted in a “messier” pattern than was observed using the edited *kkv* gene. This is presumably due to UAS-Gal4 leading to overexpression.

Methods and Materials

Fly Stocks and Genetics

Flies were grown on standard fly food. They were routinely raised at 25°C, but in some experiments, they were raised at 21°C to slow development. In other experiments we used a temperature sensitive Gal80 to limit UAS transgene expression (McGuire et al., 2004). In these experiments, the animals were grown at 21 °C or 18 °C and then at the desired stage transferred to 29.5°C to inactivate the Gal80 and induce the expression of the UAS transgene. The various RNAi inducing transgenes came either from the VDRC (Dietzl et al., 2007) or TRiP collections (Perkins et al., 2015). The VDRC lines were obtained from the VDRC (http://stockcenter. vdrc.at/control/main). The TRiP lines were obtained from the Bloomington Drosophila Stock Center (http://flystocks.bio.indiana.edu/) (NIH P40OD018537) as were many other lines used in the research (e.g. Gal4 lines, Df stocks, *kkv*^{1} carrying stock). Flies that carried a *y w sn*^{3} *f*^{36a} X chromosome were kindly provided by G. Guild. Other stocks were made by the author in his lab.

Constructs for generating transgenic lines.

UAS constructs

The UAS constructs were in the pUAST-attb vector (Bischof et al., 2007). There are 3 *kkv* mRNA isoforms that encode two distinct *kkv* proteins (Thurmond et al., 2018). All of our experiments and analyses were done with the A isoform unless stated otherwise. The C protein isoform is identical to the A isoform and both contain 1615 aa. The D isoform also contains 1615 aa but it differs from the other two proteins by 14 aa due to its mRNA containing an alternative coding exon. The 14 amino acids are found in the region bounded by aa 1277 and 1322 of the A isoform. A comparison of the sequence of the genomic *kkv* gene and the longest *kkv* cDNA (RE32455) from the Drosophila genome project revealed two putative single base pair deletions in RE32455. A comparison of conceptual translation with those of other chitin synthases showed that the genomic sequence was correct. The two single base pair deletions were repaired by site directed mutagenesis to correspond to the genomic sequence. The cDNA was amplified and fused to the coding region for Neon Green by Gibson assembly (NEB-E2611). This fusion gene was inserted into pUAST-attb using added Xho1 and Xba1 sites present in pUAST-attb and added to *kkv::NG* during construction using PCR and oligos containing the sites. This plasmid is referred to as *UAS-kkv::NG*. A similar strategy was used for the construct where the Neon Green tag was replaced by the ollas-his$_{6}$ (OH) tag. The nucleic acid sequences are provided in supplementary files S1 and S2 and the sequences of the tagged Kkv proteins are provided in files S3 and S4. *The UAS-kkv-R896K::NG* plasmid used for transgenesis was made by site directed mutagenesis of *UAS-kkv::NG*. Although an R to K substitution is generally considered a conservative substitution R896 is conserved in all chitin synthases and is thought to be at the catalytic site. In addition, the R to K change is found in the amorphic *kkv*^{1} mutation in Drosophila (Moussian et al., 2005). The same R to K mutation in yeast Chs2 resulted in a reduction to ~ 1% of normal Chs2 enzyme activity (Nagahashi et al., 1995). The Kkv-mos::NG protein differs from Kkv::NG by a series of mutations that lead to 8 amino acid changes (in the CS-C domain (pfam 03142)) that are found in several mosquito species (e.g Aedes aegypti, Aedes albopictus, Anopheles gambiae str. PEST, Culex pipiens pallens, Anopheles quadrimaculatus, Anopheles sinensis) . In Kkv-mos::NG the sequence from aa 702-909 is identical to the mosquito Chitin Synthase 1

proteins. The CS-C domain is from aa 722 to aa 904 in *kkv* and is slightly larger than a region of ScCHS2 that was shown to contain chitin synthase catalytic activity (ref). The *UAS-kkv-mos-NG* plasmid was constructed from *UAS-kkv::NG* by synthesis of the relevant region and by it being placed into *kkv-NG* by Gibson assembly (this and several other DNA manipulations were done by EpochLifeSciences). The nucleic acid sequence of *kkv-mos::NG* is provided in sequence file S5 and the protein sequence in S6.

The HDR repair constructs

The upstream, middle and downstream repair regions were synthesized by assembly of oligonucleotides by EpochLifeSciences. The segments that comprised Neon Green and smGFP-HA were obtained by PCR from plasmids obtained from Allelebiotech and Addgene (#63166) respectively, added in the correct position by Gibson Assembly. The synthesized segment included several silent mutations to prevent re-cutting by Crispr/Cas9. The repair segments were subcloned into pHD-DsRed vector (Addgene plasmid #51434). The sequences of the plasmids that contain the HDR repair constructs are provided in files S7 and S8. The sequences of the Kkv proteins encoded by the two edited genes are provided in File S9 and S10. The construction of the edited genes resulted in a two amino acid linker (AG) between the C terminal aa of kkv and the first amino acid of NG (or smFP). A carton showing the strategy is provided in Fig 1.

gRNA constructs: Two plasmids that express the needed gRNAs were made by inserting oligonucleotides (files S11) into the pCFD3-cU6:gRNA plasmid where they would be expressed from the pU6-3 promoter (Addgene plasmid #45946).

Transgenic Lines: Injections of DNA into embryos were done by Rainbow Transgenics. The UAS transgenes were injected into embryos that contained the VK00033 attp landing site (cytol location 65B2; 3L:6,442,676..6,442,676). The transgenes were marked by a w^+ gene and Go flies were crossed to w^{1118}; TM3/TM2 flies and the progeny screened for eye color. G1 male flies with eye color were crossed to w; TM3/TM6 female flies and stocks were established by crossing siblings.

The HDR construct and the gRNA constructs were both injected into *nos-Cas9* expressing embryos (injections by RainbowTransgenics). The Go flies were crossed to w; TM3/TM2 flies and the G1 flies were screened for candidate edits by the expression of DsRed. Numerous putative edits were obtained by screening for RFP expression from the PhD-Ds-red vector used for HDR. Putative edit containing flies were crossed to w; TM2/TM3 flies and stocks established by crossing siblings that contained the TM3 balancer. The Ds-Red expression was monitored and proved to be useful in later stock constructions. We also generated fly stocks where the DsRed was removed by crossing edited male flies to *hs-cre; TM3/TM2* females and then crossing *hs-cre; kkv::NG + DS-Red/TM3* males to *w; TM3/TM2* females. The progeny from this cross were screened for *TM3* (and non-*TM2*) flies that did not express Ds-Red. Stocks were established from such single male flies and characterized by PCR to insure they carried the edited Kkv-NG gene but lacked Ds-red sequences. No phenotypic differences were observed between edited flies that carried or did not carry Ds-Red. The presence of Ds-Red expression was convenient for following the edited gene in crosses and it was used for some experiments where we were not imaging an alternative red fluorescent protein or stain.

Characterization of *kkv* edits. Six independent lines were established for both types of edits. DNA was isolated from these and assayed for the correct DNA changes by PCR followed by sequencing (the oligos used for these experiments are in Table S1). Most of the lines appeared to be as designed and resulted in the in frame fusion of the C terminus of Kkv and the fluorescent protein with the designed two amino acid linker. Three *kkv-NG* and two *kkv-smGFP-HA* lines were retained and further characterized. No differences were seen between the 3 NG edits and between the 2 smGFP edits. One line of each was chosen as the standard for routine use.

Confocal Microscopy

Immunostaining of fixed pupal epidermal cells during the deposition of cuticle is complicated by the inability of the antibodies to penetrate cuticle after the early stages of its development. Thus, most of the imaging experiments we carried out on Kkv in pupae were done by in vivo imaging of Kkv::NG. In a small number of experiments we examined Kkv-NG in fixed tissue. In some we simply used the inherent fluorescence of the neon green tag (sometimes combined with phalloidin staining of actin). In others we used anti-NG immunostaining. Such tissue was only weakly fixed and we did not use animals that were older than around 48 hr after white prepupae (awp). Otherwise, immunostaining of pupal and larval tissues were done as described previously (Nagaraj and Adler, 2012). Imaging of live Kkv::NG containing pupae was done on a Zeiss 780 confocal microscope in the Keck Center for Cellular Imaging. Stained samples were examined on the same microscope.

Comparison of *kkv::NG* and *kkv::smFP*

We estimated the brightness difference between the products of the *kkv::NG* and *kkv::smFP* edited genes by live imaging both in the same confocal session using the same microscope conditions. We measured the brightness of maximal projections of both types of animals and then subtracted the background brightness. The ratio of brightness for *kkv::NG* and *kkv::smFP* was 14.7. To estimate the relative amount of the two proteins present we needed to correct for the relative brightness of the two fluorescent protein tags. We were unable to find a value for the brightness of *smFP* but we were able to find a value for the progenitor of smFP, superfolder GFP and Neon-Green (Lambert and Thorn, 2019). The relative brightness was 1.7, which gave an estimate that Kkv::NG was present in 8.65 fold higher concentration than Kkv::smFP. Assuming Kkv::smFP has the same specific activity as wild type Kkv we estimate the *kkv::smFP* cells only contain about 11% of the normal Kkv enzyme activity.

Kkv topology experiments

We obtained predictions for the number and locations of transmembrane domains from the following programs: TMHMM2.0, TMPRED, Uniprot, PHDhtm and CCTOP. The CCTOP site returned predictions for HMMTOP, Memsat, Octopus, Philius, Phobius, Pro, Prodiv, Scampi, ScampiMsa as well as CCTOP. 14 putative transmembrane domains were predicted by 13 or 14 of these 14 programs. These “consensus

sites are shown in Fig 6 and the specific TMHMM2.0 predictions are provided in Table S2. The specific amino acids predicted to be in each transmembrane domain were often shifted by a few amino acids by different programs but the putative transmembrane domains substantially overlapped.

To examine the topology of Kkv we drove the expression of *UAS-kkv-OH* or *UAS-kkv::NG* by *ptc-GAL4*. This results in a stripe of expression along the anterior/posterior compartment boundary in wing discs. Wing discs were dissected in PBS and fixed in the cold for 15'. The discs were then manually cut or punctured to ensure the apical surface of the epithelial cells was exposed to antibody. They were then incubated for 30' in PBS supplemented with 10% Sheep Serum. The discs were then stained overnight at 4^{o}C in PBS, 10% sheep serum plus the desired antibody. The discs were then rinsed 4 times in PBS and then stained with secondary antibody for 3 hrs at room temperature in PBS, 10% sheep serum plus secondary antibody. After 4 rinses in PBS the discs were washed with PBST (PBS plus .3% triton X100) followed by three additional washes in PBS. Finally the discs were mounted in ProLong Diamond. As a control several of the fixed and cut discs had PBST substituted for PBS in all steps in the experiment. The wing discs were examined on a Zeiss Axioskop II and photographed on a Spot Digital Camera (National Diagnostics).

Scanning Electron Microscopy

Wings were removed from two day old adult flies. In the experiments described in the paper the wings contained flip out clones (AyGal4) that expressed an RNAi for *kkv* (Trip line – HMC.05880). The hair phenotype overlapped with that seen previously in clones homozygous for kkv^{1} with but with a smaller fraction with the strongest phenotype (Ren et al., 2005). The wings were attached to studs with a vertical surface with conducting paint and they were then fractured with a tungsten needle. They were shadowed with platinum and examined in a Zeiss Sigma VP HD field emission Scanning Electron Microscpe (SEM) (NIH 1S10OD011966-01A1) at the University of Virginia Advanced Microscopy Facility.

Figure Legends

Figure 1. A. Models for the the relationship between Chitin Synthase and the patterned deposition of chitin. B. Cartoons showing the proteins encoded by both UAS transgenes and edited genes. The asterisks indicates the R896K mutation. C. The approach used for the editing of *kkv*. The upward arrows indicate the target locations of the two guide RNAs. The upper part of the panel shows the 3' end of *kkv.*

Figure 2. The rescue of the wing phenotype of *kkv::smFP* by the expression of a UAS transgene driven by *ap-Gal4.* A small region from the dorsal and ventral surface of the wing is shown for all genotypes. This region is from the posterior region. Note the thin bent hairs on both surfaces of the *kkv::smFP* homozygotes (EF) compared to those in wild type (AB) and *ap>kkv::NG* (CD) wings. Note the rescue in the dorsal surface of *ap>kkv::NG; kkv::smFP/Df* wings (GH). This is due to *ap* only driving expression of

781 UAS transgenes in the dorsal surface cells. Note the failure to see rescue in *ap>kkv R896K::NG;*
782 *kkv::smFP* wings (IJ) establishing that only the expression of a functional Kkv protein provides rescue.
783 The rescue with *ap>kkv mos::NG* can be seen in the image of the dorsal surface of such wings (K)
784 compared to the ventral surface (L).

785 Figure 3. Localization of Kkv in the pupal wing. A-F. In vivo images of *kkv::NG* pupal wings. All except B
786 are shown with the same microscope settings. Note the clear labeling of the hairs in wings from 42-58
787 hr. In the oldest wings the hairs are fainter and the image is from the focal plane where the pedestals
788 are obvious. We did not detect hair labeling in the youngest wings (A) unless the image was enhance by
789 brightening in ImageJ or Photoshop (B). G,H,I. Shown is a *ap-Gal4/+; UAS-kkv::NG* pupal 36 hr wing
790 fixed and F-actin stained with phalloidin (red). Note the NeonGreen is external to the F-actin. One can
791 also see that the NeonGreen signal is in the hair membrane and does not extend to the center of the
792 hair. J,K,L. A fixed 48 hr *ap-Gal4/+; UAS-kkv::NG* wing stained for both NeonGreen (J-green) and F-actin
793 (L-phalloidin - red). Note the bright disc of F-actin staining at the base of the hair is not associated with
794 an accumulation of Kkv::NG.

795 Figure 4. Localization of Kkv. A. A low magnification image of a *kkv::NG* notum. B. A higher
796 magnification image of part of a *kkv::NG* notum. Note the stripes of Kkv::NG along the proximal distal
797 axis of the bristles. The arrows point to several of the fluorescent puncta associated with the expression
798 of *kkv::NG.* C (C' and C''). A high magnification image of a bristle from a *UAS-ChtVis/+; neur-Gal4/*
799 *kkv::NG/+* bristle. Note the relatively smooth bands of chitin and the punctate stripes of Kkv::NG and
800 the association between the two. D,E,F. Two bristles from a *neur-Gal4/kkv::NG* pupae immunostained
801 for NeonGreen (green-D) and Kkv (red-F). E is the merged image and shows the high degree of co-
802 immunostaining. G,H,I. Bristles from a *neur-Gal4/kkv-OH* pupae immunostained for ollas (green-G) and
803 Kkv (red-I). H is the merged image and shows the high degree of co-immunostaining. J,K,L. A bristle
804 from a *neur-Gal4/UAS-kkv R896K::NG* pupae immunostained for NeonGreen (green-J) and Kkv (red-L). K
805 is the merged image and shows the high degree of co-immunostaining. Note the pattern of
806 accumulation of Kkv R896K::NG is quite abnormal and shows substantial bristle to bristle variation but
807 the co-localization is consistent. M,N,O. Pupal wings from *ap-Gal4/+; UAS-kkv::NG* immuostained for
808 NeonGreen (green-M) and Kkv (red-P). N is the mergred imaged and shows the high degree of co-
809 localization. P,Q,R. Pupal wings from *ap-Gal4/+; UAS-kkv R896K::NG* immuostained for NeonGreen
810 (green-M) and Kkv (red-P). N is the mergred imaged and shows the localization of the mutant protein is
811 highly abnormal but the high degree of co-localization remains.

812 Figure 5. Factors that mediate the localization of Kkv in stripes in bristles. A. A *sn f; kkv::NG* bristle by in
813 vivo imaging. The lack of the large F-actin bundles due to the loss of *sn* and *f* leads to highly abnormal
814 shape and abnormal pattering of Kkv::NG stripes. B. A *sn f;UAS-ChtVis/+; neur-Gal4/+* bristle by in vivo
815 imaging. The lack of the large F-actin bundles due to the loss of *sn* and *f* leads to highly abnormal bristle
816 shape and to abnormal patterning of chitin. C,D,E. A *sn f; UAS-ChtVis/+; neur-Gal4 kkv::NG/kkv::NG*
817 bristle by in vivo imaging. The lack of the large F-actin bundles due to the loss of *sn* and *f* leads to highly
818 abnormal shape and abnormal patterning of both chitin (C - red) and Kkv::NG (E – green) stripes. Note
819 the close association of Kkv and chitin (D- merged image, arrow) even though the pattern as a whole is
820 highly abnormal. F. A *UAS-dyl RNAi; neur-Gal4 kkv::NG/kkv::NG* thorax by in vivo imaging. Note the

821 bulged bristle (arrow) and the lack/great reduction of Kkv stripes. G A *UAS-Rab11-RNAi; neur-Gal4*
822 *kkv::NG/kkv::NG* bristle by in vivo imaging. Note the stub bristle phenotype (arrow) and the lack of
823 Kkv::NG stripes. H,I,J. A UAS-Ruby-Lifeact; *neur-Gal4 kkv::NG/kkv::NG* bristle showing the large bundles
824 of F-actin (H – red) and stripes of Kkv::NG (J – green). H', I',L' are higher magnification images where the
825 overlap between the F-actin bundles and Kkv::NG stripes is obvious. KLM. *Kkv::NG* bristles
826 immunostained with anti-Dyl antibody (K – red) and anti-NeonGreen antibody (M – green). In the
827 merged image (L) the interdigitated stripes of red and green can be seen (arrow). N-S. Orthogonal
828 cross sections of bristles of various genotypes. N. *kkv::NG* shows a distinct pattern of stripes. O. *UAS-*
829 *ChtVis/+; neur-Gal4 kkv::NG/kkv::NG* shows the close association of the chitin bands and the stripes of
830 Kkv::NG. In many cases the chitin is external to Kkv::NG (arrows). P. *UAS-Rab11-RNAi; neur-Gal4*
831 *kkv::NG/kkv::NG* bristles show a failure in the localization of Kkv to the plasma membrane. Q. *UAS-dyl*
832 *RNAi; neur-Gal4 kkv::NG/kkv::NG* bristles show much of the Kkv::NG is inserted into the plasma
833 membrane but it is not localized into the strip pattern (e.g. N). R. *sn f; kkv::NG* bristles have an
834 abnormal cross section and evidence for abnormal stripes of Kkv::NG are evident (arrows). S. *sn f; UAS-*
835 *ChtVis; neur-Gal4 kkv::NG/kkv::NG* bristles show the expected abnormal cross section shape with the
836 irregular banding of Kkv::NG and chitin. Note the close association of Kkv::NG and chitin (arrows) even
837 in these very abnormal bristles.

838 Fig 6. Topology of Kkv. A. *ptc-Gal4 UAS-kkv::NG* (or *UAS-kkv*-OH) wing discs where *kkv* is expressed in a
839 stripe immunostained with various antibodies with or without detergent treatment (PBS vs PBST). B. A
840 cartoon showing the consensus transmembrane domains as described in the Methods. The location of
841 the epitope recognized by each of the antibodies. The data indicate that the amino terminus is
842 cytoplasmic and the carboxy terminus is extracellular.

843 Fig 7. Expression of *kkv::NG* leads to fluorescent puncta in the space between the pupal cuticle and the
844 apical surface of the notum epithelial cells. A, B, C. *kkv::NG* pupae. D, E, F. Oregon R pupae. G, H, I.
845 *ap-Ga4; UAS-mCD8*-GFP. A, D and G are maximal projections of the optical stack regions that encompass
846 the notum pupal cuticle. The arrow in A and G points to a likely puncta and the arrowheads to the
847 patterned brightness seen in the pupal cuticle of animals that express a fluorescent membrane protein.
848 B, E and H are maximal projections of the optical stack regions that encompass the region between the
849 notum pupal cuticle and the upper most region of the notum epithelial cells (i.e. the bristles that extend
850 apically). Since there was no fluorescence in E we took the conservative approach of extending this
851 region of the stack by 50%. The arrows in B and H point to one of the many fluorescent puncta. C, F and
852 I are maximal projections of the optical stack regions that encompass the region of cellular material
853 including bristles, hairs and the apical surface of the notum cells. The arrows points to fluorescent
854 puncta.

855 Fig 8. Examination of *kkv* mutant clones by SEM. A. Three possible models for the phenotypic effects of
856 a *kkv* mutant cell (in green) on it and its neighbors. In the uppermost the mutant phenotype is rescued
857 by neighboring wild type cells. In the middle panel the inability to synthesize chitin results in a thinner
858 wing cuticle and this is hypothesized to be entirely cell autonomous. In the lowest most panel there is
859 partial rescue of the ability to synthesize chitin and this is graded from neighboring to mutant cell. B. A
860 relatively low magnification SEM image of a fractured adult wing that contains a clone of *kkv* mutant

cells. Arrows point to two of these. C. A region of a wing without any *kkv* clones. Note the relatively consistent cuticle thickness and the parallel layers. D. A region of a wing that contains a mutant cell (mutant hair marked by an arrow). Note how thin the mutant cuticle is (arrowhead) compared to the neighboring wild type cuticle (asterisk). Note also that there is a smooth and graded transition between the mutant and neighboring cell cuticle. E. Another example of a *kkv* mutant clone as in D.

Supplemental Figure Legends.

Fig S1. The melanotic spot phenotype. A. No melanotic spot phenotype is seen in hypomorphic *kkv::smFP/Df* flies. B. The over expression of the catalytically inactive Kkv R896K mutant driven by *ap-Gal4* results in the melanotic spot (arrow) phenotype. C. The over expression of Kkv::NG driven by *ap-Gal4* results in the melanotic spot (arrow) phenotype.

Fig S2. SEM examination of wing cuticle of edited flies. A. Flies homozygous for *kkv::smFP* show the thin bent and curved wing hair phenotype. B. *kkv::smFP/Df* flies show a slightly enhanced wing hair phenotype. C. Flies homozygous for *kkv::NG* have normal wing hairs. D. *Kkv::NG/DF* flies also have normal wing hairs. E. Oregon R wild type flies have normal wing hairs. F. Ore-R/Df flies also have normal wing hairs showing that *kkv* is not haplo-insufficient.

Fig S3. *kkv::NG* is much brighter than *kkv::smFP.* A. Image of live *kkv::NG* thorax (maximal projection) as obtained from the confocal with no modifications. The arrows point to fluorescent puncta. The image was obtained with a lower laser power than we typically used to increase the range of brightness. B image of live *kkv::smFP* as obtained from the confocal using the same settings as in A. C. The image from A brightened in Photoshop by +150. D. The image in B brightened in Photoshop by +150. E. The image in C brightened by a further +150. F. The image from D brightened by a further +150. G. The image from E with both the brightness and contrast increased by 150. H. The image from E with both the brightness and contrast increased by 150. Hairs on the notum are finally visible and a bristle is barely visible. The asterisks mark pupal cuticle. The *kkv::NG* animal was a few hrs younger (48 hr awp) than the *kkv::smFP* animal (52 hr awp). Since 52 hr animals show slightly higher fluorescence this figure slightly underestimates the difference in brightness.

Fig S4. Comparison of the subcellular localization of Kkv::NG and Kkv R896K::NG. A. Image of live 44hr ap>*kkv::NG* pupal wing. B. Image of live 44hr ap>*kkv-R896K::NG* pupal wing. C. Image of a 36hr ap>*kkv::NG* pupal wing fixed and stained with both anti-NG antibody (green) and Alexa 568 phalloidin (red) to shoe F-actin. D. Image of a 36hr ap>*kkv R896K::NG* pupal wing fixed and stained with both anti-NG antibody (green) and Alexa 568 phalloidin (red) to shoe F-actin. E. Image of a live 52 hr ap>*kkv::NG* pupal wing showing a bristle with Kkv stripes. The arrows point to shed fluorescent puncta. F. Image of a live 52 hr ap>*kkv R896K::NG* pupal wing showing a bristle with abnormal accumulation of Kkv. G. Orthogonal cross sections of bristles from *ap>kkv::NG* live pupae. H. Orthogonal cross sections of bristles from *ap>kkv R896K::NG* live pupae. Note the stripes in G and the mislocalized Kkv in H. I. A live dissected salivary gland from a *ptc-Gal4/+; UAS-kkv::NG* third instar larva. The Kkv::NG preferentially accumulates on the apical surface of the gland (arrow) next to the lumen (asterisk). I' is a blow up of a single optical

899 section of a *ptc-Gal4/+; UAS-kkv::NG* salivary gland. Note the many round vesicles with puncta obvious in
900 the membrane of these vesicles (arrow). J. A live dissected salivary gland from a *ptc-Gal4/+; UAS-kkv*
901 *R896K::NG* third instar larva. The Kkv R896K::NG does not preferentially accumulate on the apical surface
902 of the gland next to the lumen (asterisk). Rather, it is rather evenly distributed across the cytoplasm. J'.
903 The blow up shows a different morphology in how the protein accumulates compared to Kkv::NG (I').

904 Fig S5. Specificity of Kkv staining. A. A *ptc-Gal4/UAS-ChtVis; UAS-kkv::NG* wing disc shows the
905 accumulation of Kkv::NG in the *ptc* domain (arrow). The secreted ChtVis (red) diffuses all over the disc
906 in the extracellular domin that separates the disc epithelium and the peripodial membrane. B. Kkv::NG
907 preferentially accumulates on the apical surface of disc cells (arrow). C-F. Comparisons of *kkv::NG* (CE)
908 and Ore-R (DF) 63 hr awp pupae by live imaging. C and D were taken at the same microscope settings as
909 were E and F. Note the bristle, hair and cell membrane fluorescence of Kkv::NG is specific and not seen
910 in Ore-R. The arrows in C and D point to auto-flourescent pupal cuticle. E and F are higher
911 magnification images that show the stripes of Kkv::NG in bristles and the lack of such fluorescence in
912 Ore-R.
913
914 Fig S6. Kkv::NG fluorescence as a function of developmental time since white prepuae formation. All
915 images were taken at the same microscope setting.
916
917 Fig S7. How geometry affects optical sectioning of bristles. A cartoon of a bristle (B) in cross section is
918 shown with intracellular bands of red and extracellular bands of green. The arrows indicate different
919 planes of sectioning and the images the arrow point to show the expected resulting images and how
920 these can differ depending on the location and orientation of the optical sections.
921
922 Fig S8. The accumulation of Dyl in stripes in bristles is altered in sn f double mutants. A. A *sn f* bristle
923 immunostained with anti-Dyl antibodies. Note the parallel lines of Dyl staining (Nagaraj and Adler,
924 2012) are disrupted. B. Cross sections of several *sn f* bristles immunostained for Dyl. Note the
925 disruption in staining and the retention of lines of Dyl is variable from bristle to bristle.
926
927 Fig S9. Kkv::NG dependent puncta in live pupae. A. Many puncta (arrow) are visible in the space
928 between the pupal cuticle and the notum epidermis in 50 hr awp pupa. The pupal cuticle is visible
929 (asterisk) due to autoflourescence. B. Puncta are visible and concentrated along the mid line of a 20 hr
930 awp *kkv::NG* pupa. At this time the epidermal cells are still attached to the pupal cuticle they
931 synthesized so the cellular outlines are visible. C. Puncta are visible (arrow) in the space between the
932 pupal cuticle and the notum epidermis in 50 hr awp *ap-Gal4/+; UAS-kkv::NG/+* pupa. D. No puncta are
933 visible (arrow) in the space between the pupal cuticle and the notum epidermis in 50 hr awp *ap-Gal4/+;*
934 *UAS-kkv R896K::NG/+* pupa. This is likely due primarily to the protein not being localized properly to the
935 apical surface.
936
937 Fig s10. Puncta associated with pupal cuticle can be stained with both anti-NG and anti-Kkv antibodies.
938 Pupal cuticle was fixed and dissected from 42 hr *kkv::NG* pupae and immunostained with both anti-NG
939 and anti-Kkv antibodies. Many puncta were visible and a large number of these stained with both

antibodies consistent with the hypothesis that the puncta visualized by in vivo imaging of NeonGreen also contained Kkv.

Acknowledgements

This research was supported by funds provided by the W. R. Kenan Chair to the author and to a limited extent personal funds of the author. The author thanks H.S. Tzu for helpful conversations. "We acquired confocal images using the Keck Center Zeiss 780 Confocal microscopy system (NIH OD016446). We acquired Scanning Electron Microscope images at the Advanced Microscopy Facility at the University of Virginia. The images were obtained on a Zeiss VP HD SEM field purchased with a grant from the NIH (NIH 1S10OD011966).

References

Adler, P. N. (2017). Gene expression and morphogenesis during the deposition of Drosophila wing cuticle. *Fly (Austin)* **11**, 194-199.

Adler, P. N., Sobala, L. F., Thom, D. and Nagaraj, R. (2013). dusky-like is required to maintain the integrity and planar cell polarity of hairs during the development of the Drosophila wing. *Developmental biology* **379**, 76-91.

Bischof, J., Maeda, R. K., Hediger, M., Karch, F. and Basler, K. (2007). An optimized transgenesis system for Drosophila using germ-line-specific phiC31 integrases. *Proceedings of the National Academy of Sciences of the United States of America* **104**, 3312-3317.

Bouligand, Y. (1972). Twisted fibrous arrangements in biological materials and cholesteric mesophases. *Tissue Cell* **4**, 189-217.

Broehan, G., Zimoch, L., Wessels, A., Ertas, B. and Merzendorfer, H. (2007). A chymotrypsin-like serine protease interacts with the chitin synthase from the midgut of the tobacco hornworm. *J Exp Biol* **210**, 3636-3643.

Cabib, E. and Bowers, B. (1971). Chitin and yeast budding. Localization of chitin in yeast bud scars. *J Biol Chem* **246**, 152-159.

Calero-Cuenca, F. J. and Sotillos, S. (2018). Nuf and Rip11 requirement for polarity determinant recycling during Drosophila development. *Small GTPases* **9**, 352-359.

Chanut-Delalande, H., Ferrer, P., Payre, F. and Plaza, S. (2012). Effectors of tridimensional cell morphogenesis and their evolution. *Seminars in cell & developmental biology* **23**, 341-349.

Chaudhari, S. S., Arakane, Y., Specht, C. A., Moussian, B., Boyle, D. L., Park, Y., Kramer, K. J., Beeman, R. W. and Muthukrishnan, S. (2011). Knickkopf protein protects and organizes chitin in the newly synthesized insect exoskeleton. *Proceedings of the National Academy of Sciences of the United States of America* **108**, 17028-17033.

Chuang, J. S. and Schekman, R. W. (1996). Differential trafficking and timed localization of two chitin synthase proteins, Chs2p and Chs3p. *J Cell Biol* **135**, 597-610.

Devine, W. P., Lubarsky, B., Shaw, K., Luschnig, S., Messina, L. and Krasnow, M. A. (2005). Requirement for chitin biosynthesis in epithelial tube morphogenesis. *Proceedings of the National Academy of Sciences of the United States of America* **102**, 17014-17019.

Dietzl, G., Chen, D., Schnorrer, F., Su, K. C., Barinova, Y., Fellner, M., Gasser, B., Kinsey, K., Oppel, S., Scheiblauer, S., et al. (2007). A genome-wide transgenic RNAi library for conditional gene inactivation in Drosophila. *Nature* **448**, 151-156.

Dorfmueller, H. C., Ferenbach, A. T., Borodkin, V. S. and van Aalten, D. M. (2014). A structural and biochemical model of processive chitin synthesis. *J Biol Chem* **289**, 23020-23028.

Dos Santos, G., Schroeder, A. J., Goodman, J. L., Strelets, V. B., Crosby, M. A., Thurmond, J., Emmert, D. B., Gelbart, W. M. and FlyBase, C. (2015). FlyBase: introduction of the Drosophila melanogaster Release 6 reference genome assembly and large-scale migration of genome annotations. *Nucleic acids research* **43**, D690-697.

Elieh-Ali-Komi, D. and Hamblin, M. R. (2016). Chitin and Chitosan: Production and Application of Versatile Biomedical Nanomaterials. *Int J Adv Res (Indore)* **4**, 411-427.

Fernandes, I., Chanut-Delalande, H., Ferrer, P., Latapie, Y., Waltzer, L., Affolter, M., Payre, F. and Plaza, S. (2010). Zona pellucida domain proteins remodel the apical compartment for localized cell shape changes. *Dev Cell* **18**, 64-76.

Foltman, M., Filali-Mouncef, Y., Crespo, D. and Sanchez-Diaz, A. (2018). Cell polarity protein Spa2 coordinates Chs2 incorporation at the division site in budding yeast. *PLoS genetics* **14**, e1007299.

Gohlke, S., Muthukrishnan, S. and Merzendorfer, H. (2017). In Vitro and In Vivo Studies on the Structural Organization of Chs3 from Saccharomyces cerevisiae. *Int J Mol Sci* **18**.

Guild, G. M., Connelly, P. S., Vranich, K. A., Shaw, M. K. and Tilney, L. G. (2002). Actin filament turnover removes bundles from Drosophila bristle cells. *Journal of cell science* **115**, 641-653.

Hatan, M., Shinder, V., Israeli, D., Schnorrer, F. and Volk, T. (2011). The Drosophila blood brain barrier is maintained by GPCR-dependent dynamic actin structures. *J Cell Biol* **192**, 307-319.

Hernandez-Gonzalez, M., Bravo-Plaza, I., Pinar, M., de Los Rios, V., Arst, H. N., Jr. and Penalva, M. A. (2018). Endocytic recycling via the TGN underlies the polarized hyphal mode of life. *PLoS genetics* **14**, e1007291.

Jovine, L., Darie, C. C., Litscher, E. S. and Wassarman, P. M. (2005). Zona pellucida domain proteins. *Annual review of biochemistry* **74**, 83-114.

Jovine, L., Qi, H., Williams, Z., Litscher, E. and Wassarman, P. M. (2002). The ZP domain is a conserved module for polymerization of extracellular proteins. *Nature cell biology* **4**, 457-461.

Karouzou, M. V., Spyropoulos, Y., Iconomidou, V. A., Cornman, R. S., Hamodrakas, S. J. and Willis, J. H. (2007). Drosophila cuticular proteins with the R&R Consensus: annotation and classification with a new tool for discriminating RR-1 and RR-2 sequences. *Insect biochemistry and molecular biology* **37**, 754-760.

Knafler, H. C., Smaczynska-de, R., II, Walker, L. A., Lee, K. K., Gow, N. A. R. and Ayscough, K. R. (2019). AP-2-Dependent Endocytic Recycling of the Chitin Synthase Chs3 Regulates Polarized Growth in Candida albicans. *MBio* **10**.

Kozubowski, L., Panek, H., Rosenthal, A., Bloecher, A., DeMarini, D. J. and Tatchell, K. (2003). A Bni4-Glc7 phosphatase complex that recruits chitin synthase to the site of bud emergence. *Mol Biol Cell* **14**, 26-39.

Lambert, T. and Thorn, K. (2019). FPbase.org - The Fluorescent Protein Database.

Latge, J. P., Mouyna, I., Tekaia, F., Beauvais, A., Debeaupuis, J. P. and Nierman, W. (2005). Specific molecular features in the organization and biosynthesis of the cell wall of Aspergillus fumigatus. *Med Mycol* **43 Suppl 1**, S15-22.

Leal-Morales, C. A., Bracker, C. E. and Bartnicki-Garcia, S. (1994). Subcellular localization, abundance and stability of chitin synthetases 1 and 2 from Saccharomyces cerevisiae. *Microbiology* **140 (Pt 9)**, 2207-2216.

Lichtenthaler, S. F., Lemberg, M. K. and Fluhrer, R. (2018). Proteolytic ectodomain shedding of membrane proteins in mammals-hardware, concepts, and recent developments. *EMBO J* **37**.

Maue, L., Meissner, D. and Merzendorfer, H. (2009). Purification of an active, oligomeric chitin synthase complex from the midgut of the tobacco hornworm. *Insect biochemistry and molecular biology* **39**, 654-659.

McGuire, S. E., Mao, Z. and Davis, R. L. (2004). Spatiotemporal gene expression targeting with the TARGET and gene-switch systems in Drosophila. *Sci STKE* **2004**, pl6.

Merzendorfer, H. (2006). Insect chitin synthases: a review. *J Comp Physiol B* **176**, 1-15.

The cellular basis of chitin synthesis in fungi and insects: common principles and differences. *European journal of cell biology* **90**, 759-769.

Merzendorfer, H. and Zimoch, L. (2003). Chitin metabolism in insects: structure, function and regulation of chitin synthases and chitinases. *J Exp Biol* **206**, 4393-4412.

Moussian, B. (2013). The apical plasma membrane of chitin-synthesizing epithelia. *Insect science* **20**, 139-146.

Moussian, B., Letizia, A., Martinez-Corrales, G., Rotstein, B., Casali, A. and Llimargas, M. (2015). Deciphering the genetic programme triggering timely and spatially-regulated chitin deposition. *PLoS genetics* **11**, e1004939.

Moussian, B., Schwarz, H., Bartoszewski, S. and Nusslein-Volhard, C. (2005). Involvement of chitin in exoskeleton morphogenesis in Drosophila melanogaster. *Journal of morphology* **264**, 117-130.

Moussian, B., Seifarth, C., Muller, U., Berger, J. and Schwarz, H. (2006a). Cuticle differentiation during Drosophila embryogenesis. *Arthropod structure & development* **35**, 137-152.

Moussian, B., Tang, E., Tonning, A., Helms, S., Schwarz, H., Nusslein-Volhard, C. and Uv, A. E. (2006b). Drosophila Knickkopf and Retroactive are needed for epithelial tube growth and cuticle differentiation through their specific requirement for chitin filament organization. *Development* **133**, 163-171.

Moussian, B., Veerkamp, J., Muller, U. and Schwarz, H. (2007). Assembly of the Drosophila larval exoskeleton requires controlled secretion and shaping of the apical plasma membrane. *Matrix biology : journal of the International Society for Matrix Biology* **26**, 337-347.

Muszkieta, L., Aimanianda, V., Mellado, E., Gribaldo, S., Alcazar-Fuoli, L., Szewczyk, E., Prevost, M. C. and Latge, J. P. (2014). Deciphering the role of the chitin synthase families 1 and 2 in the in vivo and in vitro growth of Aspergillus fumigatus by multiple gene targeting deletion. *Cell Microbiol* **16**, 1784-1805.

Nagahashi, S., Sudoh, M., Ono, N., Sawada, R., Yamaguchi, E., Uchida, Y., Mio, T., Takagi, M., Arisawa, M. and Yamada-Okabe, H. (1995). Characterization of chitin synthase 2 of Saccharomyces cerevisiae. Implication of two highly conserved domains as possible catalytic sites. *J Biol Chem* **270**, 13961-13967.

Nagaraj, R. and Adler, P. N. (2012). Dusky-like functions as a Rab11 effector for the deposition of cuticle during Drosophila bristle development. *Development* **139**, 906-916.

Ostrowski, S., Dierick, H. A. and Bejsovec, A. (2002). Genetic control of cuticle formation during embryonic development of Drosophila melanogaster. *Genetics* **161**, 171-182.

Ozturk-Colak, A., Moussian, B., Araujo, S. J. and Casanova, J. (2016). A feedback mechanism converts individual cell features into a supracellular ECM structure in Drosophila trachea. *Elife* **5**.

Park, S. H., Cheong, C., Idoyaga, J., Kim, J. Y., Choi, J. H., Do, Y., Lee, H., Jo, J. H., Oh, Y. S., Im, W., et al. (2008). Generation and application of new rat monoclonal antibodies against synthetic FLAG and OLLAS tags for improved immunodetection. *J Immunol Methods* **331**, 27-38.

Perkins, L. A., Holderbaum, L., Tao, R., Hu, Y., Sopko, R., McCall, K., Yang-Zhou, D., Flockhart, I., Binari, R., Shim, H. S., et al. (2015). The Transgenic RNAi Project at Harvard Medical School: Resources and Validation. *Genetics* **201**, 843-852.

Polko, J. K. and Kieber, J. J. (2019). The Regulation of Cellulose Biosynthesis in Plants. *Plant Cell* **31**, 282-296.

Ren, N., Zhu, C., Lee, H. and Adler, P. N. (2005). Gene expression during Drosophila wing morphogenesis and differentiation. *Genetics* **171**, 625-638.

Riedl, J., Crevenna, A. H., Kessenbrock, K., Yu, J. H., Neukirchen, D., Bista, M., Bradke, F., Jenne, D., Holak, T. A., Werb, Z., et al. (2008). Lifeact: a versatile marker to visualize F-actin. *Nat Methods* **5**, 605-607.

Ryder, E., Ashburner, M., Bautista-Llacer, R., Drummond, J., Webster, J., Johnson, G., Morley, T., Chan, Y. S., Blows, F., Coulson, D., et al. (2007). The DrosDel deletion collection: a Drosophila genomewide chromosomal deficiency resource. *Genetics* **177**, 615-629.

Sacristan, C., Manzano-Lopez, J., Reyes, A., Spang, A., Muniz, M. and Roncero, C. (2013). Oligomerization of the chitin synthase Chs3 is monitored at the Golgi and affects its endocytic recycling. *Mol Microbiol* **90**, 252-266.

Saiz-Baggetto, S., Mendez, E., Quilis, I., Igual, J. C. and Bano, M. C. (2017). Chimeric proteins tagged with specific 3xHA cassettes may present instability and functional problems. *PLoS One* **12**, e0183067.

Santos, B. and Snyder, M. (1997). Targeting of chitin synthase 3 to polarized growth sites in yeast requires Chs5p and Myo2p. *J Cell Biol* **136**, 95-110.

Shaner, N. C., Lambert, G. G., Chammas, A., Ni, Y., Cranfill, P. J., Baird, M. A., Sell, B. R., Allen, J. R., Day, R. N., Israelsson, M., et al. (2013). A bright monomeric green fluorescent protein derived from Branchiostoma lanceolatum. *Nat Methods* **10**, 407-409.

Sobala, L. F. and Adler, P. N. (2016). The Gene Expression Program for the Formation of Wing Cuticle in Drosophila. *PLoS genetics* **12**, e1006100.

Sobala, L. F., Wang, Y. and Adler, P. N. (2015). ChtVis-Tomato, a genetic reporter for in vivo visualization of chitin deposition in Drosophila. *Development* **142**, in press.

Thurmond, J., Goodman, J. L., Strelets, V. B., Attrill, H., Gramates, L S., Marygold, S. J., Matthews, B. B., Millburn, G., Antonazzo, G., Trovisco, V., et al. (2018). FlyBase 2.0: the next generation. *Nucleic acids research* **47**, D759-D765.

Tilney, L. G., Connelly, P. S., Ruggiero, L., Vranich, K. A., Guild, G. M. and Derosier, D. (2004). The role actin filaments play in providing the characteristic curved form of Drosophila bristles. *Mol Biol Cell* **15**, 5481-5491.

Tilney, L. G., Tilney, M. S. and Guild, G. M. (1995). F actin bundles in Drosophila bristles. I. Two filament cross-links are involved in bundling. *J Cell Biol* **130**, 629-638.

Tonning, A., Hemphala, J., Tang, E., Nannmark, U., Samakovlis, C. and Uv, A. (2005). A transient luminal chitinous matrix is required to model epithelial tube diameter in the Drosophila trachea. *Dev Cell* **9**, 423-430.

Turner, C. M. and Adler, P. N. (1998). Distinct roles for the actin and microtubule cytoskeletons in the morphogenesis of epidermal hairs during wing development in Drosophila. *Mech Dev* **70**, 181-192.

van Niel, G., D'Angelo, G. and Raposo, G. (2018). Shedding light on the cell biology of extracellular vesicles. *Nat Rev Mol Cell Biol* **19**, 213-228.

Viswanathan, S., Williams, M. E., Bloss, E. B., Stasevich, T. J., Speer, C. M., Nern, A., Pfeiffer, B. D., Hooks, B. M., Li, W. P., English, B. P., et al. (2015). High-performance probes for light and electron microscopy. *Nat Methods* **12**, 568-576.

Welz, T., Wellbourne-Wood, J. and Kerkhoff, E. (2014). Orchestration of cell surface proteins by Rab11. *Trends Cell Biol* **24**, 407-415.

Willis, J. H. (2010). Structural cuticular proteins from arthropods: annotation, nomenclature, and sequence characteristics in the genomics era. *Insect biochemistry and molecular biology* **40**, 189-204.

Wong, L. L. and Adler, P. N. (1993). Tissue polarity genes of Drosophila regulate the subcellular location for prehair initiation in pupal wing cells. *J Cell Biol* **123**, 209-221.

Yabe, T., Yamada-Okabe, T., Nakajima, T., Sudoh, M., Arisawa, M. and Yamada-Okabe, H. (1998). Mutational analysis of chitin synthase 2 of Saccharomyces cerevisiae. Identification of additional amino acid residues involved in its catalytic activity. *Eur J Biochem* **258**, 941-947.

Zhang, X. and Zhu, K. Y. (2013). Biochemical characterization of chitin synthase activity and inhibition in the African malaria mosquito, Anopheles gambiae. *Insect science* **20**, 158-166.

Zimoch, L. and Merzendorfer, H. (2002). Immunolocalization of chitin synthase in the tobacco hornworm. *Cell Tissue Res* **308**, 287-297.

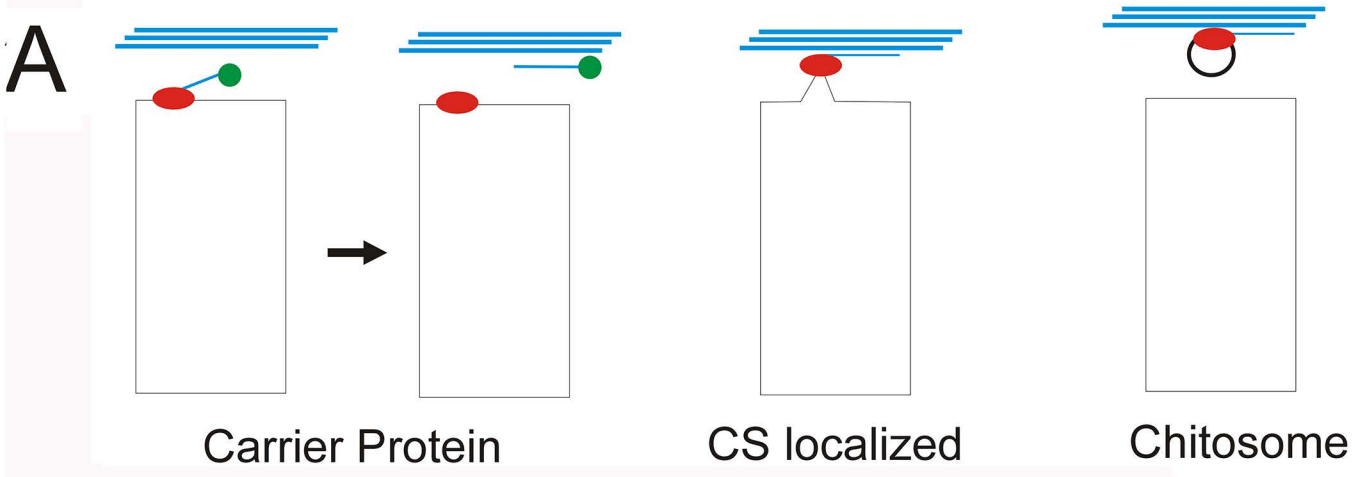
A
Carrier Protein
CS localized
Chitosome

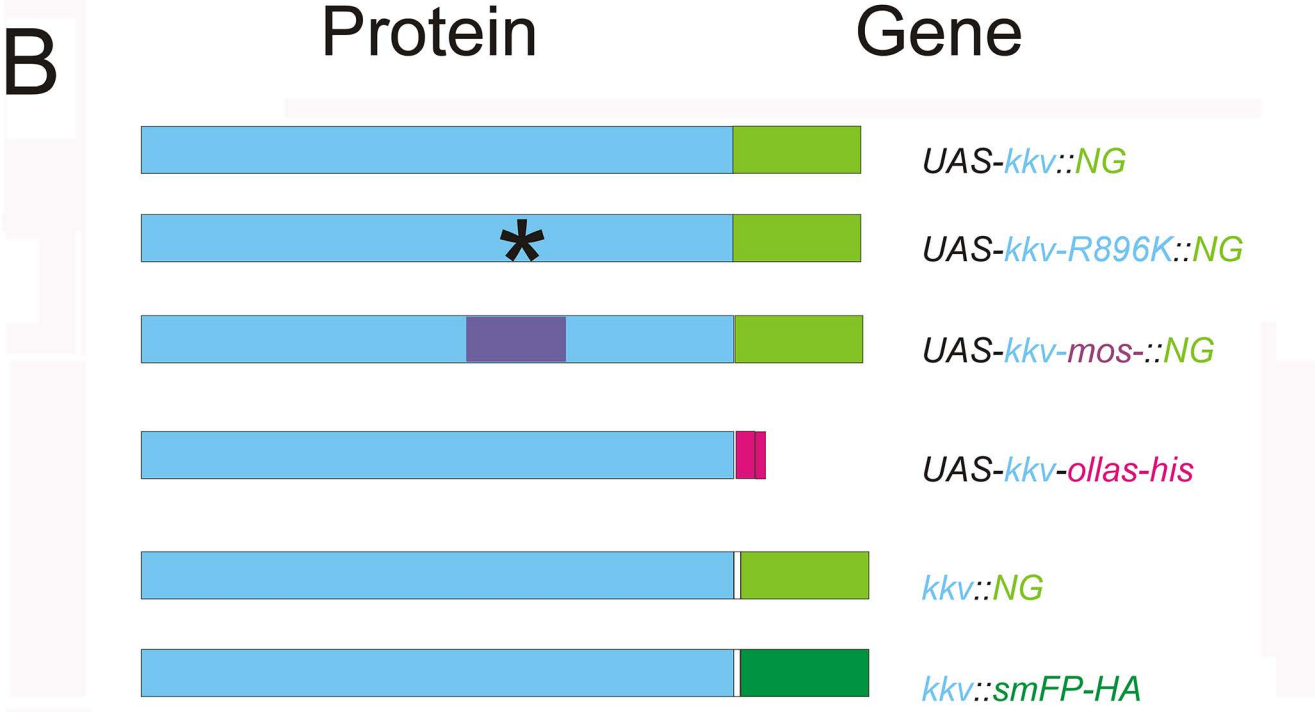
B
Protein
Gene
UAS-kkv::NG
UAS-kkv-R896K::NG
UAS-kkv-mos-::NG
UAS-kkv-ollas-his
kkv::NG
kkv::smFP-HA

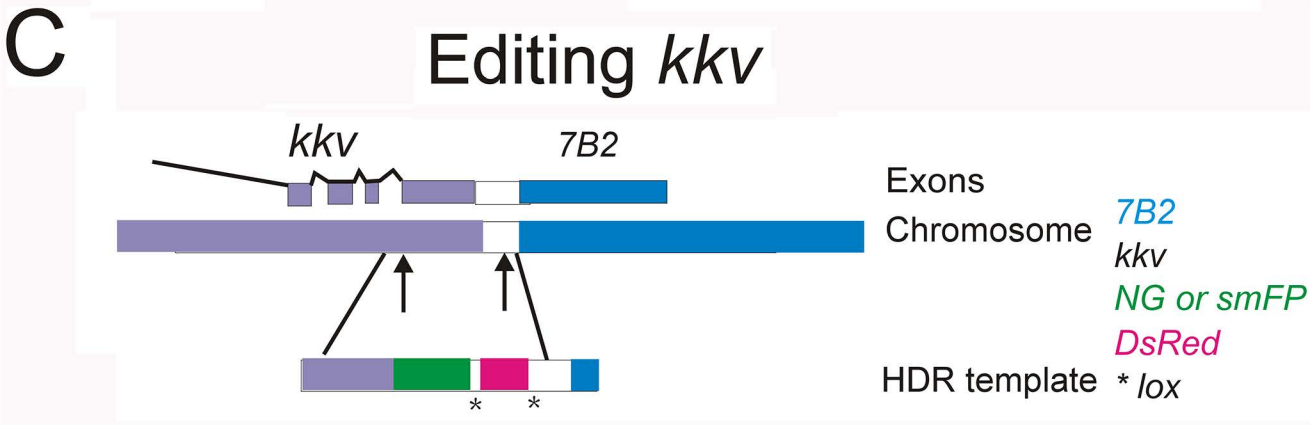
C
Editing kkv
kkv
7B2
Exons
Chromosome
7B2
kkv
NG or smFP
DsRed
HDR template
* lox

Figure 1

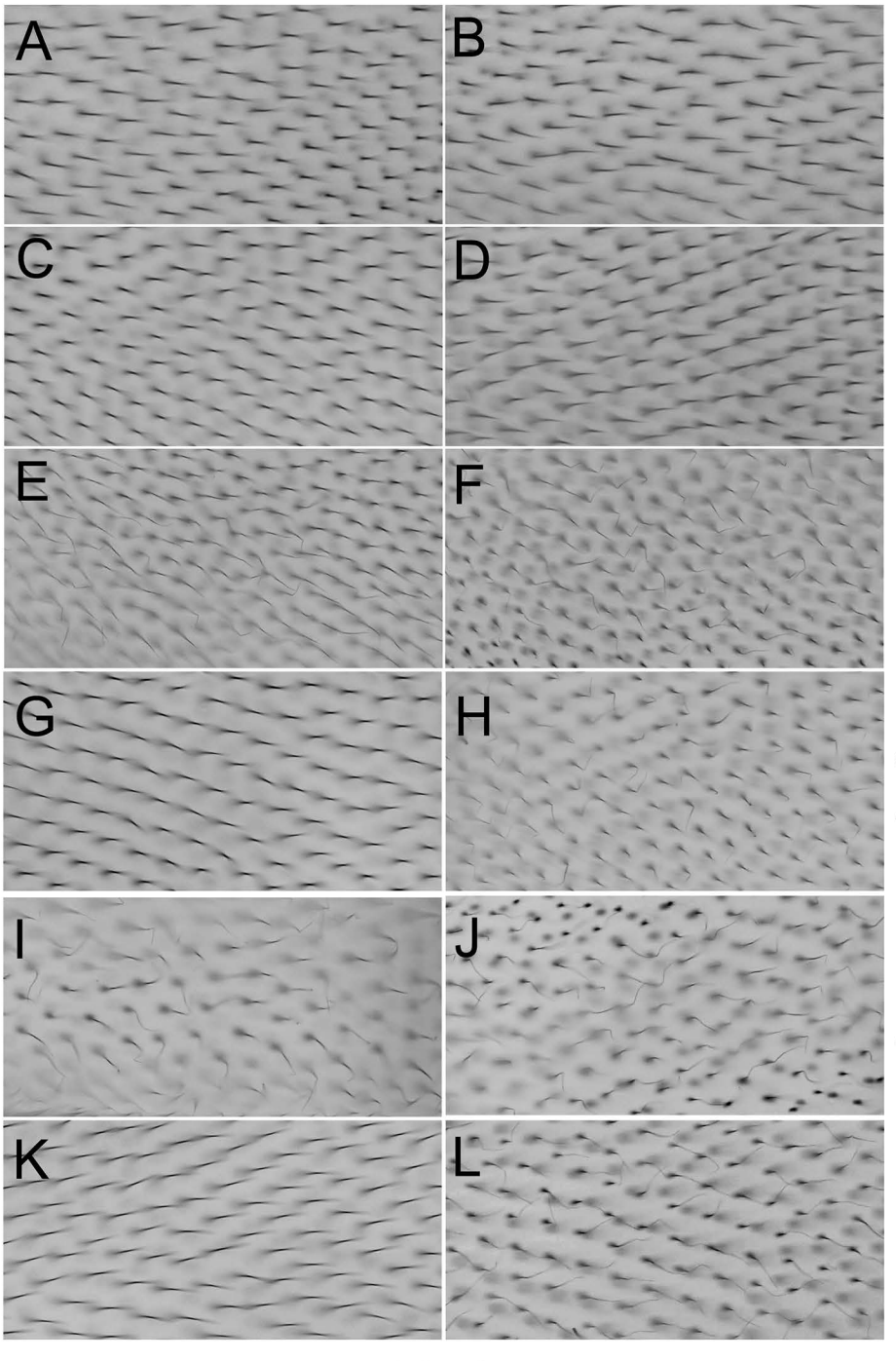
dorsal
ventral
A
B
C
D
E
F
G
H
I
J
K
L
Oregon-R
ap>UAS-kkv::NG
kkv::smFP
ap>kkv::NG; kkv::smFP/
Df(kkv)
ap>kkv R896K::NG;
kkv::smFP/kkv::smFP
ap>kkv mos::NG;
kkv::smFP/kkv::smFP

Fig 2

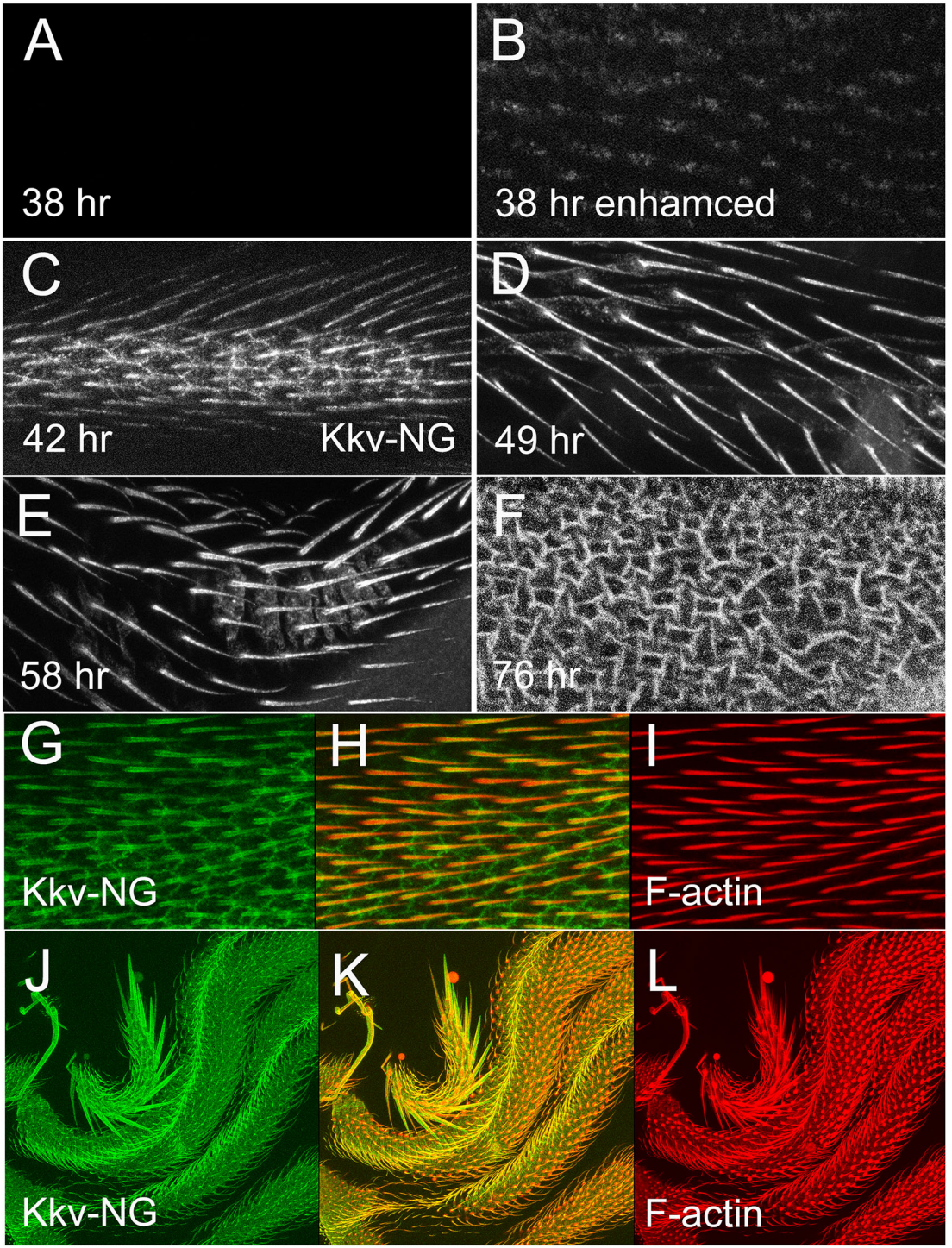
A
38 hr
B
38 hr enhamced
C
42 hr
Kkv-NG
D
49 hr
E
58 hr
F
76 hr
G
Kkv-NG
H
I
F-actin
J
Kkv-NG
K
L
F-actin

Figure 3

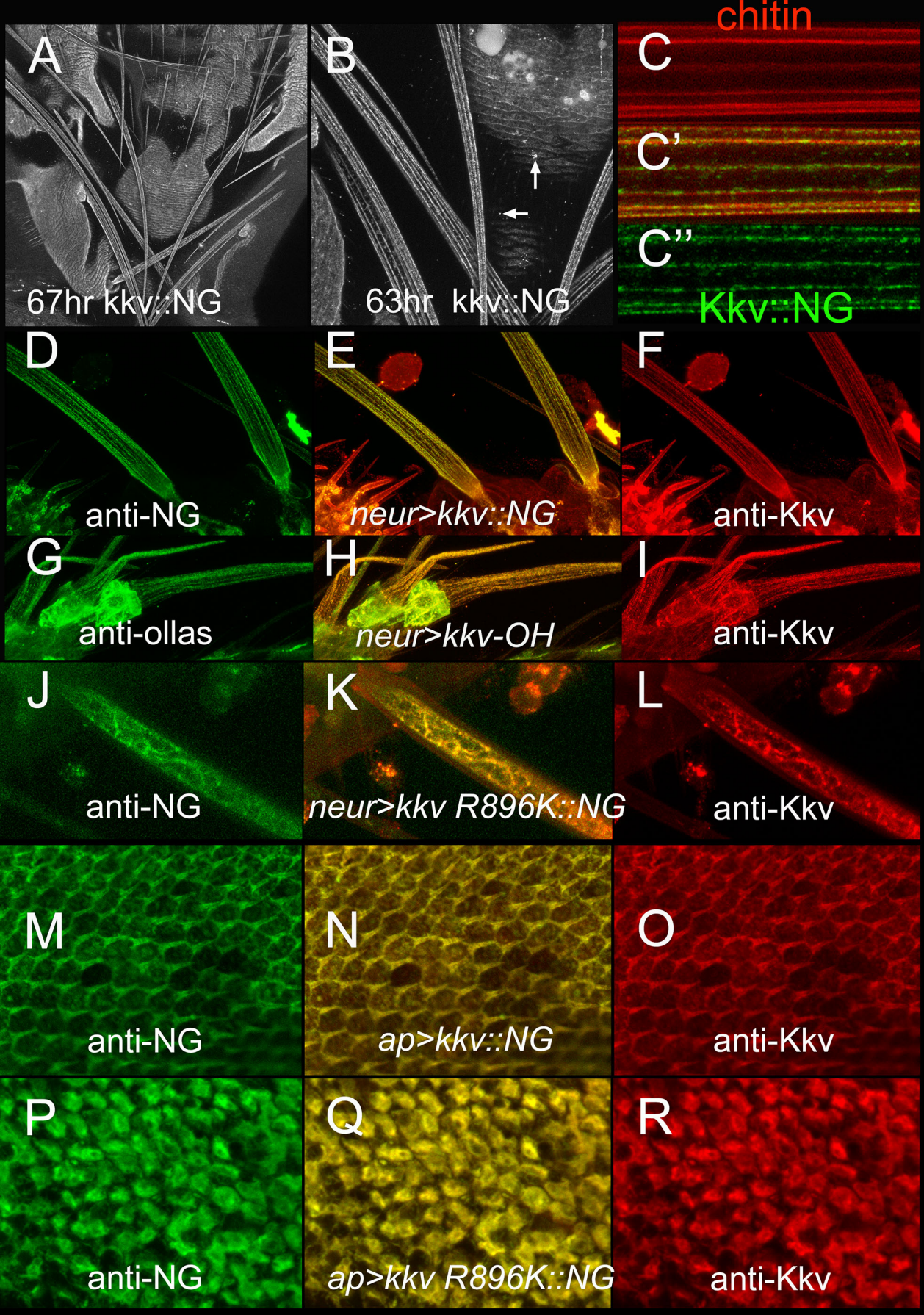
A
67hr kkv::NG
B
63hr kkv::NG
chitin
C
C'
C''
Kkv::NG
D
anti-NG
E
neur>kkv::NG
F
anti-Kkv
G
anti-ollas
H
neur>kkv-OH
I
anti-Kkv
J
anti-NG
K
neur>kkv R896K::NG
L
anti-Kkv
M
anti-NG
N
ap>kkv::NG
O
anti-Kkv
P
anti-NG
Q
ap>kkv R896K::NG
R
anti-Kkv

Figure 4

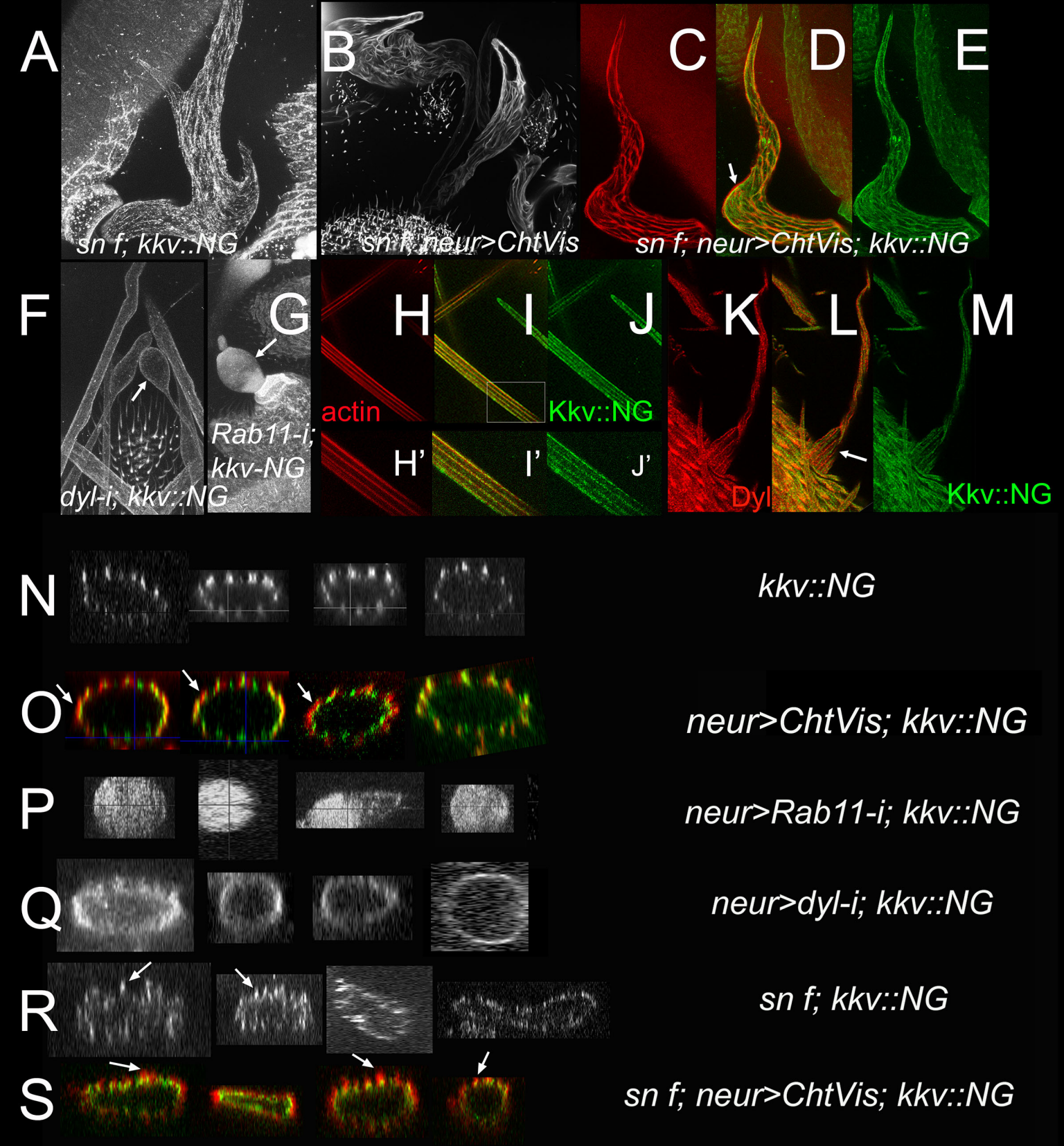
A
B
C
D
E
sn f; kkv::NG
sn f; neur>ChtVis
sn f; neur>ChtVis; kkv::NG
F
G
H
I
J
K
L
M
actin
Kkv::NG
H'
I'
J'
Dyl
Kkv::NG
Rab11-i; kkv-NG
dyl-i; kkv::NG
N
kkv::NG
O
neur>ChtVis; kkv::NG
P
neur>Rab11-i; kkv::NG
Q
neur>dyl-i; kkv::NG
R
sn f; kkv::NG
S
sn f; neur>ChtVis; kkv::NG

Figure 5

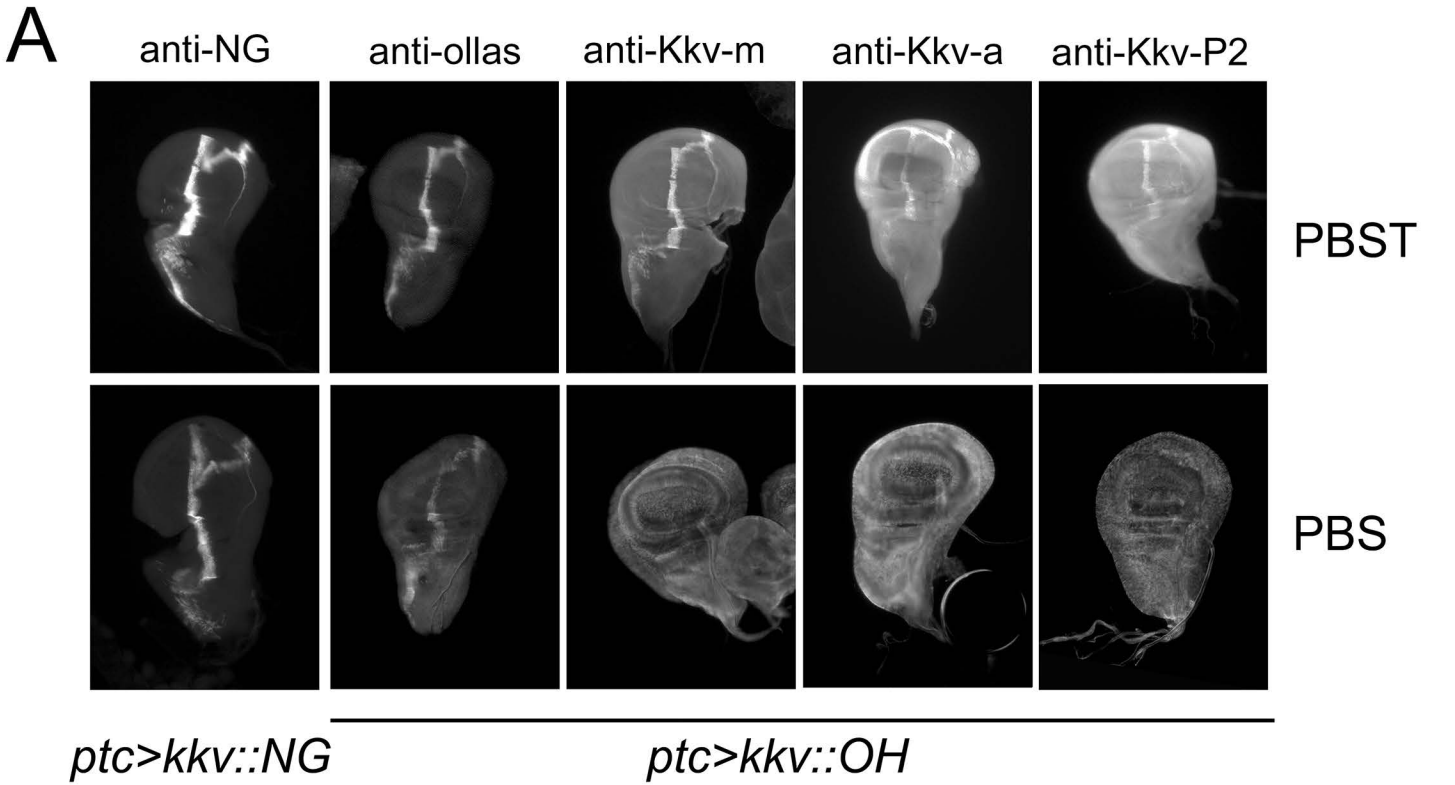
A
anti-NG
anti-ollas
anti-Kkv-m
anti-Kkv-a
anti-Kkv-P2
PBST
PBS
ptc>kkv::NG
ptc>kkv::OH
B
Kkv
0
200
400
600
800
1000
1200
1400
1600
Predicted TMD
Antibody Probes
M A P2 C

Figure 6

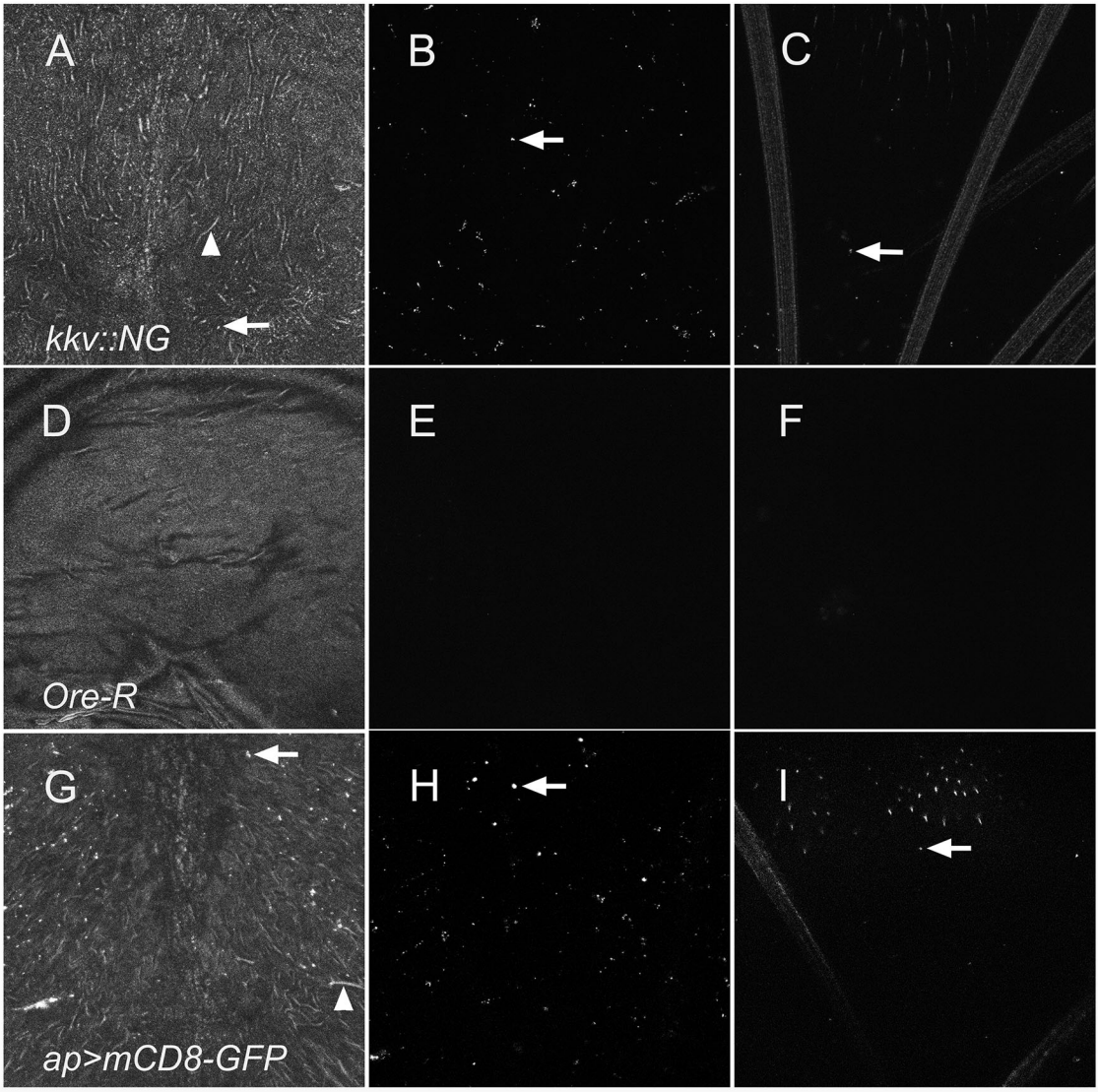

Figure 7

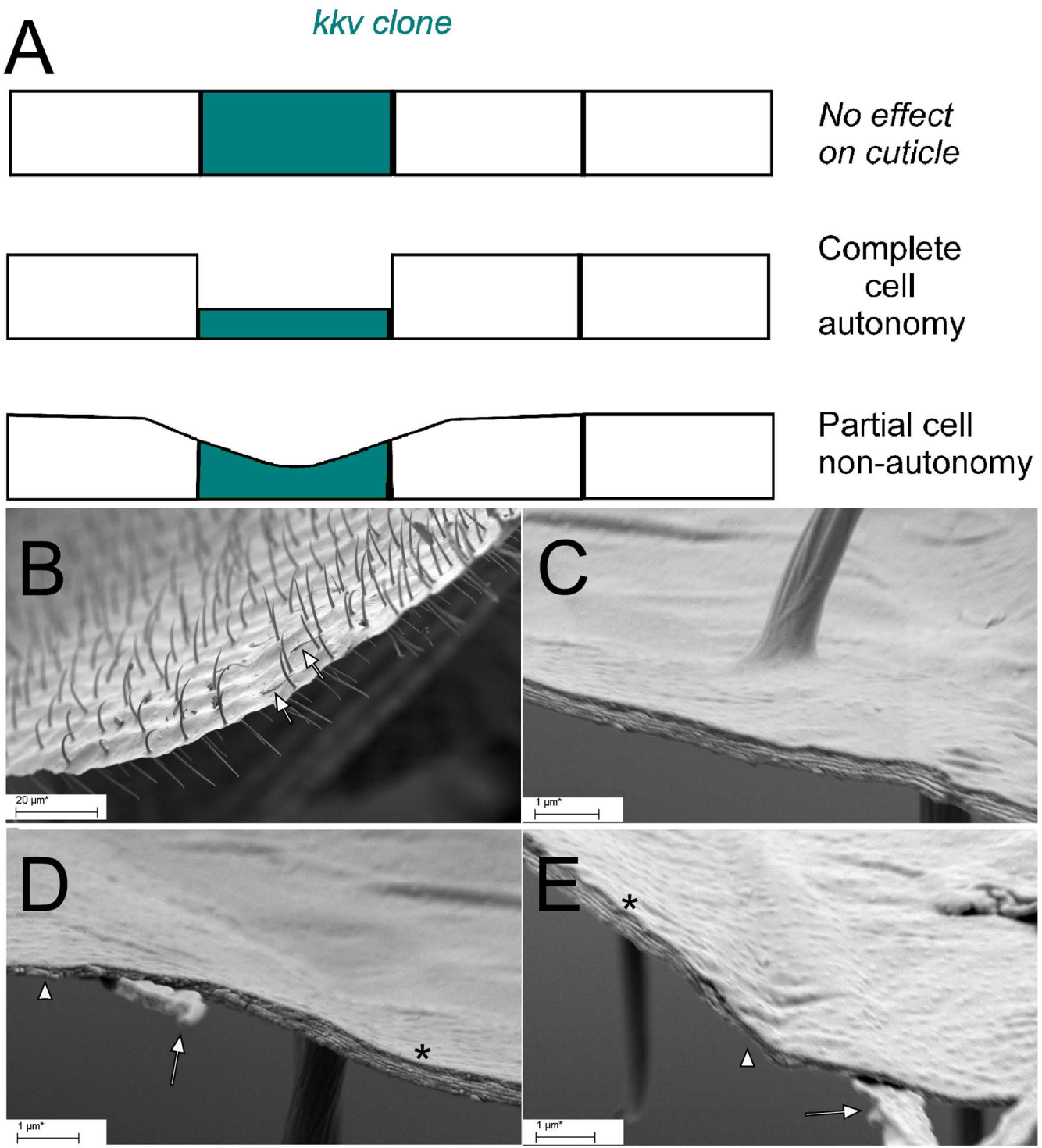
A
kkv clone
No effect on cuticle
Complete cell autonomy
Partial cell non-autonomy
B
20 µm*
C
1 µm*
D
1 µm*
E
1 µm*

Figure 8